Research Square

Preprints are preliminary reports that have not undergone peer review.
They should not be considered conclusive, used to inform clinical practice,
or referenced by the media as validated information.

# Nanoformulation of cerium oxide nanoparticles using pink pepper (Schinus terebinthifolius Raddi) for the management of type 2 diabetes

**Rosa Martha Pérez Gutiérrez**

rmpg@prodigy.net.mx

Instituto Politécnico Nacional

**Julio Téllez Gómez**

Secretaría de Ciencia, Humanidades, Tecnología e Innovación

**Alethia Muñiz-Ramírez**

Secretaría de Ciencia, Humanidades, Tecnología e Innovación

**Abraham Heriberto García-Campoy**

Secretaría de Ciencia, Humanidades, Tecnología e Innovación

**Jesus Carlos Sánchez Ochoa**

Instituto Politécnico Nacional

**Research Article**

**Keywords:** cerium nanoparticles, Schinus terebinthifoliu, anti-inflammatory, antioxidant, insulin secretion

**Posted Date:** August 27th, 2026

**DOI:** https://doi.org/10.21203/rs.3.rs-10639431/v1

**License:** This work is licensed under a Creative Commons Attribution 4.0 International License.
Read Full License

**Additional Declarations:** No competing interests reported.

## Abstract

# Background and aim

: Persistent inflammation and hyperglycemia drive insulin resistance and oxidative stress in Type 2 diabetes. Cerium oxide nanoparticles conjugated with pink pepper (ST-CeriaNP) were developed and administered to diabetic mice, aiming to boost antioxidant defenses and regulate inflammatory pathways for improved outcomes.

# Experimental procedure:

The nanoparticles were thoroughly characterized using multiple spectroscopic and microscopic techniques. Experimental diabetes was induced in male C57BL/6J mice with streptozotocin, and fasting blood glucose was tracked before and after four weeks of treatment with ST extract, cerium nanoparticles, their combination, or Metformin. Disease progression and treatment efficacy were assessed through both invasive (blood glucose, GTT, ITT) and non-invasive (urination, body weight, intake patterns) measures, ensuring a comprehensive evaluation of physiological changes and therapeutic outcomes.

# Results

ST-CeriaNP markedly attenuates hyperglycemia, reduces oxidative stress, restores antioxidant defenses, lowers lipid peroxidation, and improves insulin resistance through anti-inflammatory mechanisms. the combination of nano-cerium with *S. terebinthifolius* exhibited superior efficacy compared to individual administration, effectively mitigating type 2 diabetes. The integrated evaluation confirmed that ST/Ceria NP treatment was the most effective in alleviating diabetic symptoms, delivering synergistic benefits beyond either component alone or achieving outcomes comparable to standard Metformin therapy.

# Conclusion

The combination of cerium oxide nanoparticles with *S. terebinthifolius* extract significantly reduced hyperglycemia, oxidative stress, and lipid peroxidation, while restoring antioxidant defenses and improving insulin resistance via anti-inflammatory mechanisms. These findings highlight the potential of ST-CeriaNP as a promising nanotherapeutic strategy for the management of type 2 diabetes, warranting further investigation toward translational and clinical applications.

## Introduction

Type 2 diabetes is a complex metabolic disorder marked by chronic hyperglycemia and insulin resistance [1]. Excess glucose triggers oxidative stress, generating free radicals that damage endothelial

cells and drive vascular complications. This is worsened by advanced glycation end products (AGEs), which amplify cellular injury. Persistent hyperglycemia also promotes dyslipidemia, reflected in abnormal lipid profiles: high LDL, low HDL, and elevated triglycerides and cholesterol [2]. Chronic inflammation, though initially protective, drives the progression of diseases such as cardiovascular disorders, autoimmune conditions, cancer, and diabetes. Macrophages play a central role by releasing pro-inflammatory cytokines (IL-6, IL-1β, TNF-α) and signaling molecules. Targeting these mediators offers promising therapeutic strategies to reduce diabetes-related inflammation [3].

*Schinus terebinthifolius* Raddi, a member of the Anacardiaceae family, has emerged as a plant of considerable therapeutic interest owing to its diverse biomolecular profile [4, 7]. Its essential oil exhibits notable antioxidant activity and has been reported to attenuate memory deficits. Fruit extracts demonstrate anti-inflammatory, antioxidant, and vasoprotective properties, effectively reducing oxidative stress and vascular dysfunction [8–11]. Importantly, these extracts inhibit α-amylase and α-glycosidase enzymes, while polysaccharides contribute to antidiabetic activity through enzymatic modulation. Leaves of *S. terebinthifolius* are particularly recognized for their strong antioxidant capacity, evidenced by modulation of oxidative stress markers. These include decreased total hydroperoxides, increased sulfhydryl content, reduced malondialdehyde (MDA), enhanced catalase and superoxide dismutase (SOD) activity, and altered glutathione peroxidase (GPx) activity [12–14]. Moreover, topical applications of the leaves have demonstrated significant anti-inflammatory effects [15,16].

Cerium oxide nanoparticles ($CeO_2$ NP, or Ceria NP) are being actively studied for their enzyme-like antioxidant properties [17, 18]. Their ability to switch between $Ce^{3+}$ and $Ce^{4+}$ oxidation states allow them to sustain antioxidative activity, offering protective potential in diabetes mellitus (DM) [19].. This redox cycle underpins their therapeutic promise in diabetic models, making a review of their mechanisms and benefits crucial for future DM treatments. Previous research has shown $CeO_2$ NP effectiveness as standalone agents in Cell models (3T3-L1 adipocytes, C2C12 myotubes) and clinical applications (diabetic foot ulcers, gestational diabetes) [20–22]. However, few studies have explored their synergistic use with plant extracts, such as *Alternanthera sessilis* leaf extract, which may enhance their antidiabetic potential.

This work reports the first exploration of combining cerium oxide ($CeO_2$) nanoparticles with *Schinus terebinthifolius* to treat diabetes. Known for its antioxidant phenolic compounds, *S. terebinthifolius* helps counteract oxidative stress linked to diabetic conditions. By integrating $CeO_2$ nanoparticles with the plant extract, both in vitro and in vivo experiments demonstrated significant antidiabetic effects in type 2 diabetes models. These promising results highlight the potential of this novel strategy and support further investigation toward clinical application.

## Materials and Methods

# Chemicals and Plant material

Acrylonitrile, cerium nitrate hexahydrate, dimethyl sulfoxide, ethanol, Folin–Ciocalteu reagent, formic acid, ammonium hydroxide, MTT solution, and streptozotocin were purchased from Sigma (St. Louis, MO, USA). ELISA kits were obtained from Merck & Co., Inc (Darmstadt, Germany), Cytokine, and e-Bioscience, Inc. Fruits of pink pepper (S. terebinthifolius) were acquired from a commercial supplier, and their botanical identity was confirmed at the Herbarium of the National School of Biological Sciences, Mexico (specimen no. 78168).

## Preparation of pink pepper extract

Fresh *Schinus terebinthifolius* fruits rinsed with bidistilled water and cut into fragments. 350 g fruit extracted with 900 mL ethanol:water (1:1, v/v, Milli-Q). Extraction was performed using ultrasound-assisted system (Cole-Parmer, USA), 40 kHz, 200 W, 45°C, 30 min. Extract filtered through Whatman No. 42 paper. Yield 15% (w/w) crude extract relative to dry plant material. Liquid extracts stored short-term at 4°C in tightly sealed amber vials; avoid light, oxygen, and repeated freeze–thaw cycle

## .23Determination flavonoids and total phenolic compounds

The total flavonoid *(TP)* of the hydroalcoholic extract was quantified using a spectrophotometric assay with the Folin–Ciocalteu reagent. The method served as an initial screening tool for flavonoid which was later validated by HPLC analysis. Quercetin served as the calibration standard, and absorbance was measured at 415 nm. Results were expressed as quercetin equivalents. The determination of total phenolic compounds was carried out by preparing gallic acid standards in distilled water to construct a calibration curve (10–200 µg/mL). For each measurement, 0.5 mL of sample or standard was mixed with 2.5 mL of Folin–Ciocalteu reagent previously diluted 1:10 with water. After allowing the mixture to stand for 5 minutes, 2 mL of sodium carbonate solution was added, and the reaction was left to proceed for 30–60 minutes at room temperature in the dark. Finally, absorbance was recorded at 760–765 nm using a spectrophotometer to quantify phenolic content [23].

*Analysis of* phenolic *compounds in Schinus terebinthifolius fruits*

Phenolic compounds were analyzed using high-performance liquid chromatography (HPLC) on a Shimadzu system with a Purospher Star C18 column, employing a mobile phase of formic acid, water, and acrylonitrile under a programmed gradient. The separation was carried out at 1 mL/min, beginning with 95% solvent A and gradually shifting to 75% A / 25% B, followed by an isocratic hold and re-equilibration to initial conditions. Detection was performed at 330 nm, and tandem mass spectrometry (MS/MS) in positive ion mode was used to record product ion mass-to-charge ratios. Fragmentation patterns were compared against reference databases (PubChem, MassBank, NIST, mzCloud) to confirm compound identity.

## Synthesis of ST-ceriaNP

Ceria nanoparticles (CeriaNPs) were synthesized using a sol–gel method in which cerium nitrate hexahydrate was dissolved in Milli-Q water and adjusted to pH 7–8 with dropwise addition of $NH_4OH$. The mixture was stirred at room temperature for 24 h, during which the suspension changed color, indicating nanoparticle formation. The resulting suspension was combined with an aqueous solution of *Schinus terebinthifolius* (ST) extract and agitated for 2 h, followed by centrifugation 18, xg. for 30 minutes to remove unreacted precursors. The pellet was resuspended in Milli-Q water, dialyzed for 24 h, and stored at room temperature for subsequent use.

## Characterization of ceriaNP and ST-CeriaNP

The physicochemical characterization of cerium oxide nanoparticles (CeriaNPs) and their ST-functionalized forms (ST-CeriaNPs) was carried out using multiple analytical techniques. Particle size distribution and polydispersity index were measured by dynamic light scattering (DLS), while zeta potential was determined with a Zetasizer Nano ZSP (Malvern Instruments, Malvern, UK), at 25°C in triplicate ZSP Morphological and structural features were examined by transmission electron microscopy (TEM; HT7700, Hitachi High-Tech, Tokyo, Japan). and functional groups were identified through Fourier-transform infrared (FTIR) spectroscopy TENSOR27 spectrophotometer (Bruker, (Ettlingen, Germany). Optical properties were assessed via UV–visible absorption spectra UV-1800 spectrophotometer Shimadzu, (Tokyo, Japan)., and surface chemical composition along with oxidation states was analyzed using X-ray photoelectron spectroscopy (XPS; Thermo Fisher Scientific Inc, Ma, USA).

# Studies in vitro

# Encapsulation efficiency (EE) and loading content (LC)

In this procedure, the ST entrapment efficiency and loading content in Se NPs were measured

by a UV- visible spectrophotometer. The dried ST-CeriaNPs (40 mg) were dissolved in DMSO and centrifuged at 3000 rpm for 10 minutes. After the supernatant was collected, the absorbance was measured at 250 nm. The concentration of ST was obtained from the calibration curve

obtained in absolute ethanol (R2 = 0.9991). The drug release was quantified using the following Eq. (1):

## Drug Release Assay

The release behavior of ST from cerium oxide nanoparticles (ST-CeriaNPs) was investigated using a dynamic dialysis method under simulated physiological conditions. Three media gastric fluid (pH 5.5), intestinal fluid (pH 6.5, PBS), and plasma (pH 7.4, saline) were supplemented with Tween 80 to maintain sink conditions. ST-CeriaNPs (400 µg ST per mL) were enclosed in dialysis bags and incubated at 37°C with agitation, while free ST served as the control. Samples were periodically withdrawn, centrifuged

(12,000 rpm, 5 min), and analyzed by UV spectroscopy to quantify release. Throughout the study, nanoparticles remained in aqueous suspension, and the extract was prepared by freeze-drying to remove solvents before reconstitution in Milli-Q water.

# Cytotoxicity of STCeria nanoparticles

The cytotoxicity of ST-Ceria nanoparticles (NPs) was evaluated in RINm5f β-cells cultured under standard conditions with DMEM supplemented with serum and antibiotics. Cells were seeded at a density of $5 \times 10^4$ per well and pretreated with streptozotocin (30 μM) before exposure to varying concentrations of ST-Ceria NPs (0–300 μg/mL). Cell viability was assessed using the MTT assay, in which metabolically active cells reduced MTT to formazan crystals, later dissolved in DMSO and quantified spectrophotometrically at 570 nm. Results were expressed as the percentage of absorbance relative to untreated controls, providing a measure of nanoparticle-induced cytotoxicity.

# Assessment of RINm5f β-Cell functionality

The functional integrity of RINm5f β-cells was assessed by measuring glucose-stimulated insulin secretion following STZ-induced stress. After treatment with 3 mM STZ, cells were normalized in SAB buffer containing 2.5 mM glucose, then challenged with high glucose (16.7 mM) to stimulate insulin release. Insulin secretion was quantified using a rat insulin ELISA kit, and results were expressed relative to untreated controls. To evaluate protective effects, cells were treated with 25 μg/mL of the extract and 10 μg/mL of ST-Ceria nanoparticles, allowing assessment of β-cell functionality under oxidative and metabolic stress conditions

# ST extract and ST/Ceria NP in cytokine quantification in RAW 264.7 macrophages

Cytokine production in RAW 264.7 macrophages was assessed following established protocols to evaluate the immunomodulatory effects of ST-Ceria nanoparticles [24]. Cells were cultured in DMEM with serum, treated with ST-CeriaNPs (200 μg/mL), and then stimulated with lipopolysaccharide (1 μg/mL) for 24 h. Supernatants were collected and analyzed by ELISA to quantify levels of IL-1β, IL-6, TNF-α, IL-4, and IL-10. Comparative treatments included 100 μg/mL of the extract and 50 μg/mL of nanoparticles, enabling assessment of both pro- and anti-inflammatory cytokine responses under controlled conditions.

# In Vivo studies

# Experimental animals

Male C57BL/6J mice (7–9 weeks old, 25–30 g) were obtained from the Bioterium of the School of Biological Sciences at IPN and maintained under controlled environmental conditions (25 ± 2°C, 45 ± 10% humidity, 12 h light/dark cycle) with free access to food and water. All procedures were approved by the Ethics Committee of the Escuela Nacional de Ciencias Biológicas-IPN (Folio ENCB/CEI/045/2025) and

conducted in accordance with the NIH Guide for the Care and Use of Laboratory Animals (1985 revision) and the Mexican Official Norm NOM-062-ZOO-1999, ensuring compliance with established ethical standards.

# Induction of experimental diabetes with STZ

Diabetes was induced in male C57BL/6J mice by intraperitoneal administration of streptozotocin (40 mg/kg) freshly prepared in sodium citrate buffer (pH 4.5), given once daily for five consecutive days. To prevent acute hypoglycemia, animals received 5% glucose solution for 24 h following the final injection. Fasting blood glucose was measured from tail-tip samples using a glucometer (Accu-Chek, Roche), and mice with levels above 200 mg/dL were classified as diabetic. A total of 48 diabetic mice were then randomly assigned into six experimental groups (n = 8 per group) for subsequent studies.

Group 1 (Normal Control): Received 0.9% saline PO.

Group 2 (Diabetic Control): STZ-induced diabetic mice receiving 0.9% saline PO.

Group 3 (Diabetic + ST): Received ST at a dose of 300 mg/kg PO

Group 4 (Diabetic + Ceria NP): Received cerium oxide nanoparticles at a dose of 30 mg/kg PO.

Group 5 (Diabetic + ST-Ceria NP): Received ST-conjugated cerium oxide nanoparticles at a dose of 30 mg/kg POy.

Group 6 (Diabetic + Metformin): Received metformin at a dose of 500 mg/kg iPO.

Rodents metabolize and eliminate compounds more rapidly than humans; therefore, higher doses typically in the range of 300 to 500 mg/kg are required in animal studies to achieve effective plasma concentrations and reproduce therapeutic effects [25].

# Evaluation of lipid profile and body weight in C57BL/6J Mice

Body weight of diabetic mice was monitored weekly for four weeks, and blood samples were collected to obtain serum for lipid profile analysis. Using commercial ELISA kits, concentrations of triglycerides (TG), total cholesterol (CHOL), high-density lipoprotein cholesterol (HDL-C), and low-density lipoprotein cholesterol (LDL-C) were determined according to manufacturer instructions. Serum samples were diluted (1:25), added to antibody-coated wells alongside standards, incubated with enzyme conjugates, and developed with TMB substrate before stopping with sulfuric acid. Absorbance was measured at 450 nm, and analyte concentrations were interpolated from calibration curves and expressed in mg/dL, enabling evaluation of treatment effects with ST extract, CeriaNPs, ST-CeriaNPs, and metformin.

# Effect of ST extract, Ceria NP, STCeria NP, and Mtf on biochemical markers

Blood samples collected after treatment with ST extract, Ceria nanoparticles, ST-CeriaNPs, and metformin were centrifuged to obtain supernatants for biochemical analysis. Glucose levels were measured using an enzymatic glucose oxidase assay, insulin concentrations (Cayman Chemical, Michigan, USA),were determined with commercial kits, and glycosylated hemoglobin (HbA1c) was quantified using a BioSystem kit USA). These parameters provided a comprehensive evaluation of glycemic control and treatment efficacy under the different therapeutic conditions.

# Oxidative stress biomarker analysis

The concentrations of oxidative stress biomarkers superoxide dismutase (SOD), catalase (CAT), reduced glutathione (GSH), and malondialdehyde (MDA) were quantified in serum, pancreatic, and hepatic tissues. Measurements were performed using enzyme-linked immunosorbent assay (ELISA) kits, according the manufacturer's instructions.

# Oral glucose tolerance test (OGTT)

After four weeks of experimentation, mice underwent an oral glucose tolerance test (2 g/kg). Fifteen minutes later, they received treatments of ST extract (300 mg/kg), cerium oxide nanoparticles (50 mg/kg), or their combination (ST-Ceria NP, 50 mg/kg). Blood glucose levels were measured from tail vein samples at 0, 60, 90, and 120 minutes using a Roche Accu-Chek glucometer

# Histopathological examination

Pancreatic tissues were fixed, sectioned, and stained with H&E for microscopic examination at 40× magnification to assess histopathological changes, and the number of regenerated islets was quantified to evaluate recovery.

# Statistical Analysis

Data analysis was performed using SPSS software (version 22). Group differences were assessed using one-way analysis of variance (ANOVA), followed by Duncan's multiple range test for post hoc comparisons. Results are expressed as mean ± standard deviation (SD), and statistical significance was defined as $p < 0.05$

## Results

# Concentration of flavonoids and total phenolic compounds

An optimized ultrasound-assisted extraction (UAE) of *S. terebinthifolius* yielded 112.21 ± 4.86 µg quercetin equivalents per mg of extract, surpassing the yield from hydroalcoholic extract (93.81 ± 5.17 µg QE/mg) and showing a total phenolic content of 575.34 ± 5.19 mg GAE/g. The higher efficiency is attributed to ultrasonic waves disrupting plant cell structures, enhancing flavonoid release.

# Phenolic compound profiles

*T*he hydroalcoholic extract of *S. terebinthifolius* was analyzed using HPLC-UV-MS (Fig. 1), revealing a phenolic profile characteristic of the *Schinus* genus. The identified compounds included: Glucogallin (1), Gallic acid (2), Galloyl shikimic acid (3), Methyl gallate 3-O-β-D-glucoside isomer(4), Methyl gallate 3-O-β-D-glucoside isomer 2 (5), Methyl gallate (6), Catechin (7), Digalloyl glucose (isomers 1 and 2) (8), Digalloyl glucose isomer 2 (9), Digalloyl shikimic acid (10), Kaempferol (11), Eriodyctiol (12), Naringin (13), and Masazino-flavanone (14). Among these, Masazino-flavanone ($C_{30}H_{22}O_{10}$) was identified as the predominant compound. Other notable constituents included Galloyl shikimic acid (12) and Digalloyl glucose isomer 2 (13) (Table 1).

Table 1
Characterization of phenolic compounds from *Schinus terebinthifolius*

| Num | Rf (Min) | Formula | m/z | Compound |
|---|---|---|---|---|
| 1 | 1.6 | $C_{13}H_{16}O_{10}$ | 331,169, 153, 126, 57 | Glucogallin |
| 2 | 2.1 | $C_7H_6O_5$ | 170, 153, 126, 57 | Gallic acid |
| 3 | 2.7 | $C_{14}H_{14}O_9$ | 325, 170, 169, 125 | Galloyl shikimic acid |
| 4 | 4.6 | $C_{14}H_{18}O_{10}$ | 345, 169, 125 | Methyl gallate 3-O-β-D-glucoside isomer 1 |
| 5 | 5.1 | $C_{14}H_{18}O_{10}$ | 345, 169, 125 | Methyl gallate 3-O-β-D-glucoside isomer 2 |
| 6 | 5.7 | $C_8H_8O5$ | 184, 169, 140, 124 | Methyl gallate |
| 7 | 6.3 | $C_{15}H_{14}O_6$ | 289, 124, 123, 122, 109 | Catechin |
| 8 | 13.8 | $C_{20}H_{20}O_{14}$ | 271,211, 169, 125 | Digalloyl glucose isomer 1 |
| 9 | 14.2 | $C_{20}H_{20}O_{14}$ | 271,211, 169, 125 | Digalloyl glucose isomer 2 |
| 10 | 16.6 | $C_{21}H_{18}O_{13}$ | 478, 309, 154, 121, 95 | Digalloyl shikimic acid |
| 11 | 19.2 | $C_{15}H_{10}O_6$ | 286, 285, 258, 165, 153 | Kaempherol |
| 12 | 25.7 | $C_{15}H_{12}O_6$ | 288, 253, 179, 163, 153, | Eriodyctiol |
| 13 | 27.1 | $C_{15}H_{12}O_5$ | 272, 271, 151, 120, 119, 107 | Naringenin |
| 14 | 28.4 | $C_{15}H_{10}O_6$ | 286, 257, 93, 69 | Kaempferol |
| 15 | 29.1 | $C_{30}H_{22}O_{10}$ | 542, 415,389, 201 | Masazino-flavanone |

# UV/Vis spectrophotometry

# Intermolecular Interaction

FT-IR spectroscopy was employed to characterize the surface functional groups of CeriaNPs and to evaluate their potential interactions with bioactive compounds from *ST. Spectra* were recorded in the range of 400–4000 $cm^{-1}$ (Fig. 3A–C). The pink pepper extract spectrum exhibited characteristic absorption bands at 3367, 2921, 2875, 1721, 1612, 1456, 1359, 1255, 1177, 1079, and 1044 $cm^{-1}$. The broad band at 3367 $cm^{-1}$ corresponds to –OH stretching, while the signal at 2921 $cm^{-1}$ reflects $CH_2$ and C–H stretching of aliphatic groups. The peak at 1721 $cm^{-1}$ is attributed to C = O stretching of carbonyl groups, and the band at 1612 $cm^{-1}$ to aromatic C = C vibrations. Additional absorptions at 1456 and 1359 $cm^{-1}$ correspond to $CH_3$ bending, whereas those at 1177 and 1079 $cm^{-1}$ are associated with –C–O stretching. Notably, the signals at 1721, 1612, 1456, and 1359 $cm^{-1}$ are characteristic of flavonoid structures (Fig. 3A). The CeriaNP spectrum displayed a broad, intense band at 3367 $cm^{-1}$, assigned to O–H stretching vibrations from adsorbed water. Peaks at 1612 and 1456 $cm^{-1}$ correspond to H–O–H deformation, while the band at 1062 $cm^{-1}$ represents C–O antisymmetric stretching. A distinct absorption at 1498 $cm^{-1}$, indicative of symmetric –O–C–O stretching, confirmed the formation of CeriaNPs (Fig. 3B)

In the ST–CeriaNP spectrum, several bands present in the extract (1721, 1612, 1456, 1255, 1177, 1079, and 1044 $cm^{-1}$) disappeared, suggesting direct interactions between these functional groups and the nanoparticle surface. New peaks emerged at 1750, 1563, 1463, 1367, 1311, and 1085 $cm^{-1}$, corresponding to C–C and C–H stretching vibrations. Furthermore, shifts in band positions relative to pure CeriaNPs indicate the formation of a surface layer over the cerium oxide core. These findings strongly suggest that –OH groups from flavonoid components in the ST extract actively participate in binding to CeriaNPs (Fig. 3C).

Figure 3. FTIR spectra showing the characteristic vibrational bands of (A) Ceria nanoparticles (CeriaNP), (B) the ST plant extract, and (C) the CeriaNPs functionalized with the ST extract (ST–CeriaNP). The comparison highlights the distinct absorption peaks of each component and the shifts or overlaps observed in the composite spectrum, confirming the interaction between the nanoparticles and the extract.

# Particle size distribution

Elemental cerium was reduced to form nanoparticles, and their physicochemical properties were analyzed by DLS. Both Ceria NP and ST-Ceria NP were synthesized via the sol–gel method, yielding uniform particles with average sizes of 134.6 ± 1.21 nm and 199 ± 1.76 nm, respectively. Both exhibited negative zeta potentials (–32.2 mV and – 32.6 mV), confirming successful ST coating deposition. PDI values of 0.340 (Ceria NP) and 0.360 (ST-Ceria NP) indicated relatively homogeneous size distributions, with slightly broader dispersity in the ST-modified nanoparticles due to surface functionalization (Fig. 4).

# Transmission and scanning electron microscopy

TEM analysis showed that both CeriaNPs and ST-CeriaNPs possessed uniform spherical morphologies. CeriaNPs appeared smooth with minimal agglomeration, while ST-CeriaNPs formed small aggregates that coalesced into larger clusters. The reduced agglomeration in ST-CeriaNPs is attributed to the capping effect of the S. terebinthifolius extract, which inhibited excessive aggregation during nanoparticle nucleation and ageing (Fig. 5).

## X-ray Diffraction (XRD) characterization of STceria nanoparticles

XRD analysis of ST-Ceria nanoparticles revealed distinct crystalline peaks consistent with $CeO_2$, with a Ce:O ratio close to 1:2 /Fig. 5C). Quantitative data indicated mass percentages of 14.94% Ce and 29.42% O. Elemental mapping showed spherical to polyhedral particles with uniform composition, while EDX confirmed evenly distributed Ce, C, and O signals across nanoparticle surfaces. The absence of extraneous peaks validated the high purity of the ST-Ceria nanoparticles, ruling out contamination from synthesis precursors or substrates(Fig. 5).

Figure 5. Characterization of synthesized nanoparticles. (A) Transmission electron microscopy (TEM) image of STCeriaNP, showing spherical (B) TEM image of the composite ST/STCeriaNP, where the ceria nanoparticles (20 nm) are embedded within the starch matrix, indicating successful incorporation and stabilization. (C) X-ray diffraction (XRD) pattern of STCeriaNP, confirming the crystalline nature of the cerium oxide nanoparticles and the presence of characteristic diffraction peaks consistent with the fluorite structure of ceria

*In Vitro* studies results

# Encapsulation efficiency (EE) and loading capacity (LC)

XRD and encapsulation analysis (Fig. 6A) showed that ST loading efficiency strongly depended on the Ce/ST ratio, ranging from 82.71 ± 4.16% to 45.09 ± 2.64%, with the highest efficiency at 1:0.25. Efficiency decreased significantly as the ST proportion was reduced, while excess ST could not be absorbed by nanoparticles during centrifugation. Loading capacity (LC) varied between 46.3 ± 2.34% and 23.51 ± 1.42%, with the lowest LC at 1:0.25. Although LC increased at a ratio of 1:0.75, the improvement was not statistically significant, indicating that optimal encapsulation depends on balancing Ce/ST ratios

# ST release

# Cytotoxicity assessment of STCeria NPs (MTT Assay) summarize in paragraph

The cytotoxicity of STCeria NPs was assessed using the MTT assay in RINm5f β-cells at concentrations ranging from 0 to 300 µg/mL (Fig. 7A). Across this range, no statistically significant reduction in cell

viability was observed. Nonetheless, a dose-dependent trend emerged, with inhibition of viability increasing from 5% to 200 µg/mL to 12% at 300 µg/mL. These findings guided the selection of optimal concentrations for subsequent experiments, balancing nanoparticle safety with biological efficacy to ensure minimal cytotoxicity while preserving therapeutic potential.

# Insulin release

The protective effect of STCeriaNP against STZ-induced pancreatic β-cell injury was evaluated. Exposure to STZ resulted in a significant 47% reduction in insulin secretion at 16.7 mM glucose compared to untreated controls ($p < 0.05$). Remarkably, pre-treatment with 200 µg/mL STCeriaNP prior to STZ exposure significantly restored insulin secretion (Fig. 7B). Further analysis examined insulin release in RINm5f cells under both basal and glucose-stimulated conditions (Table 2). In the absence of glucose, STCeriaNP induced a dose-dependent increase in insulin secretion at concentrations above 40 µg/mL. Under glucose stimulation, insulin release was significantly enhanced at concentrations exceeding 20 µg/mL, also in a dose-dependent manner. Cells incubated at low glucose concentrations (3–5 mM) served as the negative control, while tolbutamide, a well-known secretagogue, was used as the positive control.

Table 2
Influences of ST, and ST/Ceria NP on insulin release in RINm5f cells in presence and absence of glucose (16.7mM)

| **Concentrations (µg/mL)** | **DMSO** | **ST** | | **ST/Ceria NP** |
|---|---|---|---|---|
| In presence of glucose (16.7mM) | | | | |
| 10 | | 1.9 ± 0.07 | 2.8 ± 0.04 | 2.9 ± 0.09 |
| 20 | | 1.9 ± 0.06 | 3.1 ± 0.05* | 4.6 ± 0.05**# |
| 40 | | 1.9 ± 0.02 | 3.9 ± 0.8** | 5.1 ± 0.8*# |
| 60 | | 1.9 ± 0.04 | 4.4 ± 0.01*# | 5.6 ± 0.01*# |
| In absence of glucose | | | | |
| 10 | | 1.9 ± 0.04 | 2.0 ± 0.04 | 2.4 ± 0.04 |
| 20 | | 1.9 ± 0.05 | 2.4 ± 0.08 | 3.4 ± 0.03* |
| 40 | | 1.9 ± 0.01 | 3.0 ± 0.2* | 4.0 ± 0.07**# |
| 60 | | 1.9 ± 0.03 | 3.4 ± 0.09**# | 4.4 ± 0.08**# |

Each value represents mean ± SD, n = 4 different test; *$p < 0.05$, **$p < 0.001$, #$p < 0.001$ vs. vehicle control

## Modulat ionof cytokine expression in LPS-stimulated RAW 264.7 macrophages

LPS stimulation markedly elevated pro-inflammatory cytokines IL-1β, IL-6, and TNF-α. Treatment with 200 µg/mL STCeriaNP significantly ($p < 0.001$) suppressed their expression by 58.2%, 48.3%, and 60.1%, respectively (Fig. 8A–E). Conversely, STCeriaNP promoted the upregulation of anti-inflammatory cytokines IL-4 and IL-10 by 39.3% and 56.2%, respectively, highlighting its dual role in attenuating inflammation while enhancing anti-inflammatory signaling

Figure 8. Modulation of Cytokine Production by STCeria Nanoparticles in LPS-Stimulated RAW 264.7 Cells. Panels show the effect of STCeria NP treatment on (A) IL-1β, (B) IL-6, (C) TNF-α (proinflammatory cytokines), and (D) IL-4, (E) IL-10 (anti-inflammatory cytokines). Cells were stimulated with LPS to induce an inflammatory response, and cytokine levels were measured after treatment. Data are expressed as mean ± SD (n = 3). Asterisks indicate statistically significant differences compared with untreated controls (*$p < 0.001$)

## Animal experiment results

# Body weight

During the first week of administration, ST did not produce significant changes in body weight ($p > 0.05$). From the second week onward, however, a progressive increase was observed, continuing through the fourth week (Table 3). Remarkably, by the third week, diabetic mice treated with STCeriaNP had regained normal body weight, which was sustained until the end of the study. At termination, body weight increases were recorded in the ST (1.36-fold), CeriaNP (1.32-fold), STCeriaNP (1.41-fold), and Mtf (1.28-fold) groups. In contrast, untreated diabetic mice exhibited a 38.5% reduction in body weight.

Table 3
Effect on weight in in T2DM mice measured at 0, 2,3 and 4 weeks after of STZ, Ceria NP, ST/Ceria NP, and Mtf treatment

| **Weeks** | | | | | |
|---|---|---|---|---|---|
| Groups | 0 | 1 | 2 | 3 | 4 |
| Control | 30.4 ± 2.86 | 31.1 ± 1.76 | 33.1 ± 3.41 | 34.0 ± 5.21 | 35.1 ± 4.44 |
| Diabetic | 31.2 ± 4.64 | 30.4 ± 4.32 | 27.6 ± 2.69 | 26.5 ± 1.75 | 25.2 ± 3.78 |
| STZ | 30.5 ± 3.19 | 31.1 ± 2.66 | 31.7 ± 4.58 | 33.4 ± 2.70 | 34.0 ± 4.12 |
| Ceria NP | 29.5 ± 3.87 | 30.5 ± 1.98 | 32.4 ± 3.16 | 32.6 ± 3.68 | 33.3 ± 3.42 |
| ST/Ceria NP | 27.2 ± 2.09 | 28.4 ± 3.57 | 31.25 ± 4.71 | 33.60 ± 2.90 | 36.10 ± 1.99 |
| Mtf | 28.3 ± 4.13 | 29.18 ± 1.34 | 30.50 ± 3.26 | 31.07 ± 1.69 | 32.20 ± 3.77 |

Weight was recorded at baseline (week 0) in week 2,3 and 4 following induction with streptozotocin (STZ) ans administration of ceria or metformin (Mtf). The data illustrates the progressive changes in weight across groups, highlighting the impact of each intervention on weight maintenance or recovery in diabetic mice.

# Effect of ST extract, Ceria NP, STCeria NP, and Mtf on biochemical parameters

Diabetic mice exhibited mean hyperglycemia levels that were 3.32-fold higher than those of the control group. After one month of treatment, glycemia was significantly reduced by ST extract, Ceria NP, STCeria NP, and Mtf, with inhibition rates of 53%, 49%, 60%, and 32%, respectively. Serum insulin and HOMA-IR are critical indicators of diabetes progression. As shown in Table 4, plasma insulin and HOMA-IR levels were markedly reduced in STZ-induced diabetic mice compared to controls ($p < 0.001$). Treatment with the tested agents significantly elevated these parameters, supporting the hypothesis that the diabetic model exhibits pronounced insulin resistance. Table 4 also highlights the anti-diabetic effect of STCeria NP on HbA1c levels. HbA1c was significantly ($p < 0.001$) (elevated in diabetic mice relative to controls; however, treatment with STCeria NP effectively reduced HbA1c, suggesting its potential role in mitigating glycated hemoglobin accumulation in experimental diabetes.

Regarding lipid metabolism, diabetic mice exhibited significantly elevated serum TC, LDL-C, and TG levels, accompanied by a marked reduction in HDL-C compared with controls ($p < 0.001$). Treatment with ST extract, Ceria NP, or STCeria NP effectively reduced TC, LDL-C, and TG while increasing HDL-C, with STCeria NP producing the most pronounced improvement (Table 4). Within 14 days, diabetic mice also showed evidence of severe liver injury, reflected by markedly elevated AST, ALT, SGOT, and SGPT levels ($p < 0.05$). Administration of ST extract, Ceria NP, STCeria NP, and Mtf significantly lowered these hepatotoxicity biomarkers, indicating a protective effect on liver function. Among the interventions, STCeria NP demonstrated the strongest hepatoprotective activity, followed by ST extract and Ceria NP (Table 4).

Table 4
Effect of ST extract, Ceria NP, STCeria NPs and Mtf on Serum biochemical parameters against streptozotocin-induced diabetes in C57BL/6 J mice

| Groups | Control | Diabetic | ST extract | ceria NP | ST/ceria NP | Mtf |
|---|---|---|---|---|---|---|
| **Serum** | | | | | | |
| Glucose (mmol/L) | 4.9 ± 0.99*## | 16.3 ± 3.51* | 7.5 ± 1.56**# | 8.3 ± 1.21*** #### | 6.4 ± 0.87**## | 11.1 ± 1.56**### |
| Insulin (m/Ul) | 20 ± 2.41### | 14 ± 1.56* | 18.7 ± 1.78## | 17 ± 2.31 | 19 ± 3.05### | 18.6 ± 1.78## |
| HOMA-IR | 4.35 ± 0.75## | 10.14 ± 1.24 | 6.23 ± 0.93***## | 6.27 ± 1.46***## | 5.4 ± 0.84**## | 9.1 ± 1.24***#### |
| HbA1c (%) | 4.5 ± 0.16### | 6.1 ± 0.76** | 5.2 ± 0.53*## | 5.4 ± 0.38*## | 4.7 ± 0.29*### | 5.1 ± 0.48*## |
| **Lipid Profiles** | | | | | | |
| Total cholesterol (mg/ dL) | 70.5 ± 2.87## | 127.4 ± 5.29** | 96.2 ± 2.78*# | 101.0 ± 3.89*# | 76.5 ± 4.75## | 87.7 ± 4.12***# |
| HDL-C (mg/ dL) | 47.0 ± 4.52# | 28.6 ± 2.43** | 39.6 ± 3.90*## | 34.2 ± 4.11**### | 45.3 ± 3.38# | 38.7 ± 2.84*## |
| LDL-C (mg/ dL) | 6.8 ± 1.12## | 16.3 ± 2.41*** | 8.9 ± 0.99**# | 9.4 ± 0.66*### | 7.3 ± 0.76## | 8.8 ± 0.99**# |
| Triglyceride (mg/ dL) | 80.4 3.82### | 141.5 ± 3.70** | 91.2 ± 3.19*## | 95.3 ± 5.06*## | 84.1 ± 2.83### | 90.3 ± 2.65*## |
| **Liver profiles** | | | | | | |
| AST (mg/ dL) | 90.7 ± 5.12## | 188.5 ± 6.03** | 108.1 ± 3.97*** | 116 .4 ± 2.87***# | 95.2 ± 5.42# | 114.7 ± 4.82***# |
| ALT (mg/dL) | 60.1 ± 2.48# | 180.7 ± 2.48** | 81.4 ± 1.98*## | 88.5 ± 2.48**## | 73.3 ± 3.49### | 83.2 ± 2.67*## |
| SGOT (IU/L) | 125.6 ± 6.18# | 260.1 ± 2.48*** | 142.2 ± 4.47# | 156.3 ± 3.87# | 132.5 ± 4.97## | 148 .4 ± 2.98# |
| SGPT (IU/L) | 90.6 ± 6.18# | 161.3 ± 5.90** | 110.4 ± 2.79*## | 121.3 ± 4.32*** | 97.6 ± 5.38# | 118.7 ± 9.12***## |

Values are expressed in mean ± S.D (n = 8). Values of *p < 0.05, **p < 0.01, and ***p < 0.001 vs with normal control; p < 0.05, ##p < 0.01, and ###p < 0.001 vs diabetic mice. HOMA-IR values were calculated:

(mmol/L)×insulin (mIU/L)/22.5. Glutamate oxaloacetate transaminase (SGOT), serum glutamate pyruvate transminase (SGPT) and alkanine phosohatase (ALP), aspartate amino transferase (AST).

Oxidative stress induced by STZ was characterized by a significant reduction in antioxidant enzymes (SOD, CAT, and GSH) and a marked increase in MDA levels (Table 5). To assess the extent of this imbalance, enzymatic activity was measured in serum, pancreas, and liver samples. Notably, STCeria NP treatment enhanced antioxidant enzyme activity while reducing MDA concentrations across all three tissues ($p < 0.01$). $p < 0.05$. Comparative analysis among treated groups, normal controls, and the STZ-induced diabetes group revealed that STCeria NP consistently produced superior biochemical outcomes relative to Mtf, underscoring its efficacy in mitigating oxidative damage associated with STZ-induced type 2 diabetes.

Table 5

Effects of ST extract, Ceria nanoparticles, ST/Ceria NP combination, and Metformin (Mtf) on antioxidant levels in serum, pancreas, and liver of streptozotocin (STZ)-induced diabetic C57BL/6J mice.

| Groups | Control | Diabetic | ST extract | Ceria NP | ST/CeriaNP | Mtf |
|---|---|---|---|---|---|---|
| **Antioxidant in serum** | | | | | | |
| SOD (U/mg protein) | 10.2 ± 3.45$^{\#\#}$ | 5.4 ± 4.57** | 8.1 ± 2.35*$^{\#\#}$ | 7.6 ± 2.74***$^{\#\#}$ | 8.9 ±3.02$^{\#\#}$ | 7.7 ± 1.74***$^{\#\#}$ |
| CAT(U/mg protein) | 54.3 ± 1.89$^{\#}$ | 16.0 ± 2.22* | 46.7 ± 1.89**$^{\#\#\#}$ | 39.3 ± 1.89**$^{\#\#\#}$ | 50.5 ± 1.36$^{\#}$ | 44.3 ± 2.83**$^{\#\#\#}$ |
| GSH (mM/mg protein) | 0.82 ± 0.04$^{\#\#\#}$ | 0.31 ± 0.02*** | 0.62 ± 0.03**$^{\#}$ | 0.58 ± 0.01**$^{\#}$ | 0.74 ± 0.04$^{\#\#\#\#}$ | 0.63 ± 0.05**$^{\#}$ |
| MDA(nM/mg protein) | 3.1 ± 0.21$^{\#\#}$ | 14.3 ± 1.39*** | 4. 6 ± 0.62*$^{\#}$ | 5.6 ± 0.87**$^{\#\#\#}$ | 3.7 ± 0.42$^{\#\#}$ | 4.3 ± 0.79*$^{\#}$ |
| **Antioxidant in pancreas** | | | | | | |
| SOD (U/mg protein) | 18.5 ± 1.38 $^{\#}$ | 7.5 ± 1.12** | 13.4 ± 2.59***$^{\#\#}$ | 12.3 ± 0.97**$^{\#\#}$ | 16.8 ± 2.71$^{\#}$ | 11.51 ± 3.06**$^{\#\#}$ |
| CAT(U/mg protein) | 39.7 ± 4.24$^{\#}$ | 11.2 ± 1.84* | 29.7 ± 1.39**$^{\#\#}$ | 26.4 ± 2.54**$^{\#\#}$ | 34.7 ± 4.14***$^{\#}$ | 28.4 ± 3.21**$^{\#\#}$ |
| GSH (mM/mg protein) | 31.3 ± 4.24$^{\#}$ | 12.1 ± 4.58$^{\#}$ | 23.6 ± 2.77$^{\#}$ | 19.9 ± 1.84$^{\#}$ | 29.5 ± 3.21$^{\#}$ | 17.9 ± 3.37$^{\#}$ |
| MDA(nM/mg protein) | 1.6 ± 0.54$^{\#}$ | 8.0 ± 0.89** | 2.7 ± 0.82*$^{\#\#}$ | 3.5 ± 0.63*** $^{\#\#\#}$ | 1.8 ± 0.578$^{\#}$ | 3.1 ± 0.95*$^{\#\#}$ |
| **Antioxidant in liver** | | | | | | |
| SOD (U/mg protein) | 12.2 ± 016 $^{\#\#}$ | 4.9 ± 0.18* | 8.3 ± 0.53**$^{\#\#\#}$ | 6.1 ± 0.41** $^{\#\#\#}$ | 10.3 ± 0.28$^{\#\#}$ | 7.7 ± 0.42 **$^{\#\#\#}$ |
| CAT(U/mg protein) | 30.1 ± 1.39$^{\#}$ | 11.2 ± 2.15 | 23.8 ± 3.46**$^{\#\#\#}$ | 19.7 ± 3.61**$^{\#\#\#}$ | 26.9 ± 2.74*$^{\#\#}$ | 20.81 ± 1.45**$^{\#\#\#}$ |
| GSH (mM/mg protein) | 33.5 ± 1.90$^{\#\#}$ | 11.9 ± 0.89 | 25.1 ± 0.74*$^{\#\#\#}$ | 21.3 ± 3.04*$^{\#\#\#}$ | 29.8 ± 1.56**$^{\#}$ | 23.6 ± 2.37*$^{\#\#\#}$ |
| MDA(nM/mg protein) | 2.2 ± 0.17$^{\#}$ | 5.0 ± 0.39** | 2.0 ± 0.21**$^{\#}$ | 2.4.± 0.33**$^{\#}$ | 1.6 ± 0.14**$^{\#}$ | 1.9 ± 0.25**$^{\#}$ |

Antioxidant levels were measured in serum, pancreas, and liver homogenates. Values are expressed as mean ± standard deviation (SD), with *n = 8* animals per group. Statistical significance *p < 0.05, **p < 0.01, ***p < 0.001 compared with normal control group. #p < 0.05, ##p < 0.01, ###p < 0.001 vs. diabetic group

# Effect of ST, CeriaNP, and STCeriaNP administration on glucose intolerance in STZ-induced diabetic mice

The oral glucose tolerance test (OGTT), conducted over a 120 minutes expressed the effects of ST extract, CeriaNP, and their combination (STCeriaNP) on blood glucose regulation. Treatment with STCeriaNP significantly reduced blood glucose levels at 30, 60, and 90 minutes (p < 0.05), exhibiting a stronger hypoglycemic effect than either ST extract or CeriaNP alone. In contrast, untreated diabetic mice maintained elevated glucose levels throughout the 120-minute OGTT (Table 6).

Table 6
Effect of (A) hydroalcoholic extract of ST, Ceria NP and STCeria NPs on oral glucose tolerance (OGTT) in STZ-induced diabetic mice at 0, 30, 60, 90, and 120 min

| **Serum glucose levels (mg/dL)** | | | | | |
|---|---|---|---|---|---|
| Time (min) | | | | | |
| Time (min) | 0 | 30 | 60 | 90 | 120 |
| Control | 98 ± 4.12 | 153 ± 3.48*** (1.56-fold) | 126 ± 41.72* (1.28-fold) | 97 ± 1.83*** | 95 ± 2.90** |
| Diabetic | 271 ± 5.31 | 438 ± 7.18 (1.61-fold) | 395 ± 5.95 (1.45-fold) | 325 ± 6.48 (1.20-fold) | 263 ± 4.59 |
| D + ST extract | 214 ± 3.83 | 340 ± 8.23 (1.9-1.59-fold) | 290 ± 5.67 (1.35-fold) | 177 ± 7.13*** ( -17.3%) | 158 ± 5.89** ( -26.1%) |
| D+$Ce0_2$ NP | 232 ± 5.12 | 360 ± 6.19 (1.52-fold) | 318 ± 4.75 (1.37-fold) | 201 ± 3.86*** ( -13.3%) | 188 ± 7.11** ( -19 ± 3%) |
| D + ST/$Ce0_2$ NP | 209 ± 6.45 | 300 ± 3.50** (1.43-fold) | 272 ± 5.30** (1.30-fold) | 164 ± 2.27** (-21.5% ) | 130 ± 6.72* ( -38%) |

Values are expressed in mean ± S.D (n = 8). Values of *p < 0.05, **p < 0.01, and ***p < 0.001 vs vs diabetic mice at the same time.

# Effect of STCeriaNP on pancreatic islet pathology

Streptozotocin (STZ)-induced diabetic mice displayed severe structural damage in pancreatic islets (Fig. 9). Administration of STCeriaNP mitigated necrosis and decreased cellular degeneration, thereby preserving islet architecture and pancreatic integrity ($p < 0.05$). This protective effect underscores STCeriaNP potential of to counteract STZ-induced pancreatic injury in diabetic mice.

Figure 9. Effect of STCeriaNP on pancreatic tissue (H&E staining, X400): (A) Normal pancreas showing intact islet architecture and abundant β-cells (highlighted in green). (B) Diabetic pancreas with marked reduction in islet size and β-cell population (green circle), reflecting impaired insulin-producing capacity. (C) Diabetic mice treated with STCeriaNP exhibit restoration of islet morphology and recovery of functional β-cells (green circle), indicating the therapeutic potential of STCeriaNP in reversing pancreatic damage.

# Discussion

Type 2 diabetes is a multifactorial disorder characterized by persistent hyperglycemia and poor therapeutic control, often leading to complications. The pancreas plays a central role in glucose sensing and insulin regulation. Current research highlights natural agents with bioactive compounds as safe modulators of glycemia, while cerium oxide nanoparticles (CeNPs) are gaining attention for their potent antioxidant activity through regenerative $Ce^{3+}/Ce^{4+}$ redox cycling. This enables efficient free radical scavenging, though the exact mechanisms by which CeNPs protect pancreatic β-cells from oxidative damage remain unresolved [26].

In this study, cerium nanoparticles were successfully synthesized using $NH_4OH$ as the reducing agent and *Schinus terebinthifolius* extract as the capping agent, resulting in highly amorphous, spherical structures. UV–Vis analysis confirmed nanoparticle formation, while FT–IR data revealed stabilization through carbonyl and carboxyl group interactions from flavonoids, which facilitated coordination polymer formation and enhanced stability for drug delivery. Conjugation with *S. terebinthifolius* improved biocompatibility, binding efficiency, particle size uniformity (199 ± 1.76 nm), and reduced polydispersity (–12.6 mV). These physicochemical modifications promoted superior dissolution and controlled release under mildly acidic nasal conditions. Overall, the optimized ST–CeriaNP formulation exhibited synergistic antidiabetic activity, highlighting its potential as an effective therapeutic strategy [27].

Structural characterization confirmed the successful synthesis and functionalization of the nanoparticles (Fig. 5). XRD spectra revealed three distinct diffraction peaks corresponding to stoichiometric cerium planes, while XDX analysis detected Ce atoms along with C and O signals, indicating biomolecule capping on the nanoparticle surface. TEM imaging showed spherical morphology with uniform size distribution (Fig. 5), consistent with previous biomedical CeNP reports[28]. The nanoparticles exhibited strong plasmonic properties, highlighting their potential for colorimetric sensing due to high absorption and scattering efficiency. Additionally, ST release was slower at neutral pH compared to acidic conditions, and the ST–CeriaNPs demonstrated favorable swelling behavior, validating their effectiveness as nanocarriers.

Phytochemical studies of *Schinus terebinthifolius* reveal a rich spectrum of polyphenols with strong antidiabetic potential. Compounds such as glucogallin and gallic acid protect against diabetes-related complications and regulate insulin function through antioxidant and anti-inflammatory pathways enhances the expression of SOD, HO-1, and Nrf2 in the brains of chronically diabetic rats [29,30]. Methyl gallate enhances neural antioxidant defenses[31], while catechin improves insulin sensitivity and mitochondrial activity[32]. Eriodyctiol modulates incretin hormones (GIP, GLP-1) and suppresses pro-inflammatory cytokines [33], and naringenin promotes skeletal muscle glucose uptake [34]. Naringin reduces hepatic and renal gluconeogenesis by inhibiting key enzymes [35], and kaempferol protects against diabetic cardiomyopathy by limiting oxidative stress, apoptosis, and fibrosis [36]. Collectively, these polyphenols act through diverse molecular mechanisms to improve glucose metabolism, insulin regulation, and tissue protection in diabetes.

Untreated diabetic animals showed elevated glucose and HbA1c with reduced insulin compared to healthy controls. Treatment with ST-CeriaNP significantly normalized glucose and insulin levels ($p < 0.001$), increasing insulin up to 1.18-fold. This hypoglycemic effect likely involves stimulation of residual pancreatic β-cell insulin secretion, supported by phenolic compounds in *S. terebinthifolius*. The protective action of ST-CeriaNP against STZ-induced β-cell damage, through mitigation of oxidative stress, underpins its ability to restore insulin function and reduce hyperglycemia (Table 4). ST–CeriaNP demonstrated potent antioxidant and antidiabetic effects, significantly lowering serum glucose, LDL cholesterol, and atherogenic indices, thereby supporting long-term glycemic control and survival. Untreated diabetic mice showed persistent hyperglycemia, metabolic disturbances, and progressive body weight loss (up to 19.23%) due to β-cell destruction (Table 3), dehydration, and catabolism of fats and proteins. In contrast, ST–CeriaNP treatment promoted substantial recovery, with body weight increasing 1.32-fold, highlighting its protective and restorative capacity against diabetes-induced metabolic damage.

For the first time, ST–CeriaNP was shown to improve glucose tolerance by reducing postprandial hyperglycemia caused by glucose overload. Oral administration in STZ-diabetic mice produced a significant antihyperglycemic effect, comparable to tolbutamide treatment (Table 5), which supports pancreatic and liver regeneration reflected in serum biochemical parameters. This response reflects enhanced insulin secretion by pancreatic β-cells under glucose stimulation, further promoted by bioactive compounds such as gallic acid [30], catechin [32], eriodyctiol [36], and naringenin [37]. Untreated diabetic animals showed elevated glucose and HbA1c with reduced insulin compared to healthy controls(Table 4). Treatment with ST–CeriaNP significantly restored glucose and insulin to near-normal levels ($p < 0.001$), increasing insulin up to 1.18-fold. This hypoglycemic effect likely involves stimulation of residual pancreatic β-cell insulin secretion [12], aided by phenolic compounds in *S. terebinthifolius* (Table 1). The protective action of ST–CeriaNP against STZ-induced β-cell damage (Fig. 7),, through mitigation of oxidative stress, underpins its ability to elevate insulin and reduce blood glucose [38].

STZ is highly destructive to pancreatic β-cells, causing necrosis and impaired function. However, in this study insulin levels did not decline significantly in the STZ-only group, suggesting residual compensatory activity [39]. Diabetes is characterized by insulin resistance, which elevates lipid concentrations and promotes oxidative modification of lipoproteins, stimulating cholesterol and triglyceride synthesis. Concurrently, reduced glucose utilization by erythrocytes drives diabetic models into hyperlipidemia, reinforcing metabolic dysfunction [40]. In STZ-induced diabetic mice, dyslipidemia was marked by elevated TC, LDL-C, and triglycerides with reduced HDL-C, reflecting β-cell damage and oxidative stress. Treatment with ST–CeriaNP significantly restored lipid balance, showing stronger therapeutic effects than metformin, likely through improved glucose utilization and lipogenic activity. Elevated aminotransferases (AST, ALT, SGOT, SGPT) indicated STZ-related hepatotoxicity, with enzyme leakage into the bloodstream (table 4) [41, 42]. Both ST–CeriaNP and metformin reduced these enzyme levels, reversing hyperglycemia-induced hepatic damage. Overall, ST–CeriaNP demonstrated potent lipid-lowering and hepatoprotective effects, underscoring its promise as a therapeutic agent in diabetes management.

In STZ-induced diabetic mice, oxidative stress was evident through reduced CAT and SOD activity and elevated MDA levels. Treatment with ST–CeriaNP restored antioxidant enzyme activity, lowered MDA, and, together with ST extract, enhanced ROS scavenging and glucose regulation. Depletion of GSH, linked to lipid peroxidation and hepatocyte damage, was reversed by oral ST–CeriaNP, administration (table 4). which markedly increased GSH in serum, pancreas, and liver. These findings highlight its strong role in alleviating oxidative stress, protecting β-cells, and promoting GSH biosynthesis [43].

Cerium oxide ($CeO_2$) nanoparticles, combined with bioactive compounds from the ST extract, exhibit dual functionality by uniting the intrinsic redox properties of nanoceria with plant-derived antioxidants. Their ability to alternate between $Ce^{3+}$ and $Ce^{4+}$ states grant potent antioxidant activity [44], mimicking enzymes such as superoxide dismutase and catalase, thereby scavenging ROS linked to diabetes. This synergy enhances therapeutic potential, as $CeO_2$ nanoparticles not only reduce oxidative stress and protect pancreatic β-cells but also attenuate chronic inflammation through immune modulation and improve glucose metabolism by inhibiting α-glucosidase and promoting insulin sensitivity.

Chronic inflammation, closely linked to oxidative stress in type 2 diabetes, drives β-cell dysfunction and insulin resistance through pro-inflammatory cytokines such as IL-1, IL-6, IL-8, IL-12, IL-18, IF-γ, and TNF-α. This cascade promotes β-cell death and islet fibrosis [45]. Intervention with ST–CeriaNP, particularly via IL-1 receptor antagonism, has been shown to normalize blood glucose, enhance insulin secretion, and reduce inflammation-induced damage(Fig. 8). These findings underscore its therapeutic potential to restore β-cell function, support cell survival, and mitigate diabetes-related inflammatory progression [46]. In vitro and animal studies demonstrate that ST/Ceria nanoparticles exert potent antioxidant and anti-inflammatory effects, improving glucose metabolism, lipid profiles, and liver enzyme activity. They enhance insulin sensitivity, stimulate insulin secretion, and promote β-cell regeneration and islet restoration. By reducing oxidative stress, preserving β-cell mass, and attenuating inflammation, they achieve better glycemic control. This dual mechanism antioxidant protection from $CeO_2$ nanoparticles

and gene regulation by flavonoids highlights their therapeutic potential. The synergistic combination of CeNPs with *S. terebinthifolius* phytocompounds emerges as a promising nanomedicine strategy for diabetes management

## Conclusion

Type 2 diabetes treatment often relies on drugs with adverse effects, underscoring the need for innovative therapies. This study explored the antidiabetic potential of biosynthesized cerium nanoparticles with pink pepper (STCeriaNP) through in vitro and in vivo models. STCeriaNP improved insulin secretion and sensitivity reduced oxidative stress and inflammation, regulated body weight, normalized liver enzymes, and enhanced lipid profiles. This represents the first evidence of antidiabetic efficacy for pink pepper–mediated cerium nanoparticles, highlighting their synergistic antioxidant and anti-inflammatory mechanisms. While results are promising, limited mechanistic detail and translational scope call for further research on molecular pathways, metabolite profiling, and long-term safety to advance clinical application.

## Declarations

# Declaration of competing interest

The authors declare no conflicts of interest

# Author Contribution

R.M.P.G. and J.T.G. contributed to the study conception and experimental design. R.M.P.G. and A.M.R. performed the preparation and phytochemical characterization of the Schinus terebinthifolius extract and contributed to the synthesis and characterization of the cerium oxide nanoparticles. J.T.G. and J.C.S.O. conducted and evaluated the in vitro and in vivo experiments, including the biochemical, antioxidant, inflammatory, and histopathological analyses. A.H.G.C. contributed to the physicochemical characterization and interpretation of the nanoparticle data. R.M.P.G., A.M.R., and J.C.S.O. contributed to data analysis and statistical evaluation. R.M.P.G. and J.T.G. drafted the manuscript. A.M.R., A.H.G.C., and J.C.S.O. critically reviewed and edited the manuscript. All authors contributed to the interpretation of the results, approved the final version of the manuscript, and agreed to be accountable for all aspects of the work.

## References

1. Lee, J., Yun, J. S., Lee, S. H., Yun, J., & Ko, J. S. (2022). S.H. Advanced glycation end products and ¿their effect on vascular complications in type 2 diabetes mellitus. *N*utrients 95. https://doi.org/10.3390/nu14153086

2. Cavalli, N. P., de Mello, M. B., Righi, N. C., Schuch, F. B., Signori, L. U., & da Silva, A. M. V. (2024). Effects of high-intensity interval training and its different protocols on lipid profile and glycemic control in type 2 diabetes: A meta-analysis. *Journal Of Sports Sciences*. https://doi.org/10.1080/02640414.2024.2330232
3. Wojdasiewicz, P., Ła, P., & Szukiewicz, D. (2014). The role of inflammatory and anti-inflammtory ytokines in the pathogenesis of osteoarthritis. *Mediators Inflam*. https://doi.org/10.1155/2014/561459
4. Yedjou, C. G., Grigsby, J., Mbemi, A., Nelson, D., Mildor, B., Latinwo, L., & Tchounwou, P. B. (2023). The management of diabetes mellitus using medicinal plants and vitamins. *International Journal Of Molecular Sciences*. https://doi.org/10.3390/ijms24109085
5. Yong, P. H., New, S. Y., Azzani, M., Wu, Y. S., Chia, V. V., Ng, Z. X.. Potential of medicinal plants to ameliorate neovascularization activities in diabetes: A systematic review. Endocr. Regul., Yahia, Y., Feriani, A., Labidi, A., Ghazouani, L., & Nasri, N. (2024). (2018).Schinus terebinthifolius vs Schinus molle: location on the phytochemical content of fruits. Ind. Crop. Prod. https://doi.org/10.1016/j.indcrop.2018.05.080.
6. Schulze-Kaysers, N., Feuereisen, M. M., & Schieber, A. (2015). Phenolic compounds in edible species of the Anacardiaceous family a review. *Rsc Advances*. /https://doi.org/10.1039/C5RA11746A. https://doi.org.
7. Todirascu-Ciornea, E., El-Nashar, H. A. S., Mostafa, N. M., Eldahshan, O. A., Boiangiu, R. S., ritcu, L., & Singab, A. N. B. (2019). Schinus terebinthifolius Essential oil attenuates scopolamine-induced memory deficits via cholinergic modulation and antioxidant properties in a zebrafish model. *Evid Based Complement Iternat Med*https://doi.org/doi: 10.1155/2019/5256781
8. Feriani, A., Tir, M., Arafah, M., Gómez-Caravaca, A. M., Contreras, M. D. M., & Nahdi, S. (2021). Schinus terebinthifolius fruits intake ameliorates metabolic disorders, inflammation, xidative stress, and related vascular dysfunction, in atherogenic diet-induced obese rats.Insight of their chemical characterization using HPLC-ESI-QTOF-MS/MS. J Ethnopharmacol. https://doi.org/10.1016/j.jep.2020.113701
9. Feriani, A., Tir, M., Mufti, A., Caravaca, A. M. G., Contreras, M. D. M., Taamalli, A., Carretero, A. S., Aldawood, N., Nahdi, S., Alwasel, S., Harrath, A. H., & Tlili, N. (2021). HPLC-ESI-QTOF-MS/MS profiling and therapeutic effects of Schinus terebinthifolius and Schinus molle fruits: investigation of their antioxidant, antidiabetic, anti-inflammatory and antinociceptive properties. Inflammopharmacology. https://doi.org/10.1007/s10787-021-00791-1
10. Ferian, A., Tir, M., Hamed, M., Sila, A., Nahdi, S., Alwasel, S., & Tlili, N. (2020). Multidirectional insight solysaccharides from Schinus terebinthifolius and Schinus molle fruits: Physicochemical and functional profiles, in vitro antioxidant, anti-genotoxicity, antidiabetic, and antihemolytic capacities, and in vivo anti-inflammatory and anti- nociceptive properties. *Intern J Biol Macromol*. https://doi.org/10.1016/j.ijbiomac.2020.10.123
11. Dedvisitsakul, P., Watla-Iad, K., & Heliyon (2022). https://doi.org/10.1016/j.heliyon.2022.e10740

12. Dos Santos, P. R., de Araújo, B. A. P., do Carmo, V. M., Carollo, C. A., da Silva, D. B., Estevinho, L. M., Dos Santos, E. L., & de Picoli, S. K. (2019). Microbiological quality, chemical profile as well as antioxidant and antidiabetic activities of Schinus terebinthifolius Raddi. *Comp Biochem Physiol C*. https://doi.org/10.1016/j.cbpc.2019.02.007
13. de Oliveira, I. M., & Aroeira, A. (2020). fruit (Schinus terebinthifolius Raddi) as a natural antioxidant: Chemical constituents, bioactive compounds and in vitro and in vivo antioxidant capacity. *Food Chemistry*. https://doi.org/10.1016/j.foodchem.2020.126274
14. Nascimento, S., Péligris, H., Fabiula, F., Andrea, Y. V., Shan, R. G., & Luciana, A. N. (2023). Schinus terebinthifolius Raddi (Brazilian pepper) leaves extract: in vitro and in vivo evidence of anti–inflammatory and antioxidant properties. Inflammopharmacology. https://doi.org/10.1007/s10787-023-01316-8
15. Rosas, E. C. M., Correa, L. B., Pádua, L. A., Moreira, T. E., Mazzei, J. L., Heringer, A. P., Bizarro, C. A., Kaplan, M. A., Figueiredo, R., & Henriques, M. G. (2015). Anti-inflammatory effect of Schinus terebinthifolius Raddi hyro alcoholic extract on neutrophil migration in zymosan-induced arthritis. J. Ethnopharmacol. https://doi.org/.
16. 1016/j.jep.2015.10.014.
17. Nickerson, K., & Flory, S. L. (2001). Competitive and allelopathic effects of the invasive shrub Schinus terebinthifolius (Brazilian peppertree). *Biological Invasions*. https://doi.org/10.1007/s10530-014-0756-8
18. Regina, G. D., & Sueli, O. S. L. (2025). Nanoparticles with Antioxidant ctivity. ntioxidants. https://doi.org/.
19. 3390/antiox14020221.
20. Sura, A. S. Cerium oxide nanoparticles role as antioxidant. (2024). J. Babylon. https://doi.org/.
21. 4103/MJBL.MJBL_1022_23.
22. Amaya, L. J., Alfredo, M., Andoni, U., Silvia, L. C., & Pedro, G. M. (2019). Cerium Oxide Nanoparticles regulate insulin sensitivity and oxidative markers in 3T3-L1 Adipocytes and C2C12 myotubes. Oxidative medicin. *Cell Longevity*, *2695289*, 10. pages https://doi.org/10.1155/2019/2695289
23. Horatian, X., Tingetin, X., Fang, S., Yi, R., Jingsi, J., Le, K., Zhang, Z., & Xin, M. (2023). Cerium oxide nanoparticles in diabetic foot ulcer management: Advances, limitations, and future directions. *Colloid Surfaces B: Biointerf*. https://doi.org/10.1016/j.colsurfb.2023.113535
24. Xinyuan, L., Wanbo, Z., Rui, L., Guolian, D., & Hefeng, H. (2024). Cerium oxide nanozymes improve skeletal muscle function in gestational diabetic offspring by attenuating mitochondrial. ACS Omega. https://doi.org/.
25. 1021/acsomega.3c09025.
26. Nicolescu, A., Bunea, C. I., & Mocan, A. (2025). Total flavonoid content revised: An overview of past, present, and future determinations in phytochemical analysis. *Analytical Biochemistry*. https://doi.org/10.1016/j.ab.2025.115794

27. Lyu, S., & Park, W. (2005). Production of cytokine and NO by RAW 264.7 macrophages and PBMC in vitro incubition with flavonoids. *Archives Of Pharmacal Research*. https://doi.org/10.1007/BF02977761
28. Manickam, R. S. I. D., Presley, H., & Farid, M. (2025). Biosynthesis of cerium oxide nanoparticles using Alternanthera sessilis leaf extract and evaluation of their antioxidant, antibacterial, anti-inflammatory, antidiabetic and cytotoxic activities. *Biomedical Materials*. https://doi.org/10.7/s44174-025-00294-5
29. Zhai, J. H., Wu, Y., Wang, X. Y., Cao, Y., Xu, K., Xu, L., & GuoY. (2016).. Antioxidation of cerium oxide nanoparticles to several series of oxidative damage related to type ii diabetes mellitus in vitro. Med Sci Monit. https://doi.org/.
30. 12659/msm.901068.
31. Zhao, F., Wang, J., Zhang, Y., Hu, J., Li, C., Liu, S., Li, R., & Du, R. (2024). In vivo fate of targeted drug delivery carriers. *International Journal Of Nanomedicine*. https://doi.org/10.2147/IJN.S465959
32. Lohitha, T., & Albert, H. (2025). Biosynthesis, structural, spectroscopic, photoluminescence, and antifungal activity of ni- doped CeO2 Nanoparticles. *J Fluoresce*. https://doi.org/10.1007/s10895-024-03831-5
33. Khan, A. N., Singh, R., Bhattacharya, A., Chakravarti, R., Roy, S., & Ravichandiran, V. (2022). Ghosh, D. A Short Review on Glucogallin and its Pharmacological Activities. Mini Rev Med Chem. https://doi.org/.
34. 2174/1389557522666220513150907.
35. Xu, Y., Tang, G., Zhang, C., Wang, N., & Feng, Y. (2021). gallic acid and diabetes mellitus: its association with oxidative stress. *Molecules*. https://doi.org/10.3390/molecules26237115
36. Abdel-Hamed, A. R., Mehanna, E. T., Hazem, R. M., Badr, J. M., Abo-Elmatty, D. M., Abdel-Kader, M. S., & Goda, M. S. (2002). Plicosepalus acacia extract and its major constituents, methyl gallate and quercetin, potentiate therapeutic angiogenesis in diabetic hind limb ischemia:HPTLC quantification and LC-MS/MS metabolic profiling. *Antioxidants (Basel)*. https://doi.org/10.3390/antiox10111701
37. Wen, L., Wu, D., Tan, X., Zhong, M., Xing, J., Li, W., Lim, D., & Cao, F. (2022). The The Role of Catechins in Regulating diabetes: an update review. Nutrients.https://doi.org/10.3390/nu14214681
38. Islam, A., Islam, M. S., Rahman, M. K., Uddi, M. N., & Akanda, M. R. (2020). The pharmacological and biological roles of eriodictyol. *Archives Of Pharmacal Research*. https://doi.org/10.1007/s12272-020-01243-0
39. Alam, M. A., Subhan, N., Rahman, M. M., Uddin, S. J., Reza, H. M., & Sarker, S. D. (2014). Effect of citrus flavonoids, naringin and naringenin, on metabolic syndrome and their mechanisms f action. *Adv Nutr*. https://doi.org/10.3945/an.113.005603
40. Sundaram, R., Shanthi, P., & Sachdananda, P. (2014). Effect of tangeretin, a polymethoxylated flavone on glucose metabolism in streptozotocin-induced diabetic rats. *Phytomedicine*, *21*(2), 793–799.
41. Yang, Y., Che, Z., Zhao, X., Xie, H., Du, L., Gao, H., & Xie, C. (2022). Mechanisms of Kaempferol in of diabetes: A comprehensive and latest review. *Front Endocrinol (Lausanne*.

https://doi.org/10.3389/fendo.2022.990299

42. Guillet, C. (2010). Implication des produits terminaux de glycation dans les complications liées au Diabète. *Nutr Clin Métabolisme*. https://doi.org/10.1016/j.nupar.2010.07.002
43. D'Amico, M., Marfella, R., Nappo, F., DiFilippo, C., De Angelis, L., Berrino, L., Rossi, F., & Giugliano, D. (2001). High glucose induces ventricular instability and increases vasomotor tone in rats. Diabetologia. https://doi.org/.
44. 1007/s001250051644.
45. Ramesh, B., Saravanan, R., & Pugalendi, K. V. (2005). Influence of Sesame Oil on Blood Glucose, Lipid Peroxidation, and Antioxidant Status in Streptozotocin Diabetic Rats. *Journal Of Medicinal Food*. https://doi.org/10.1089/jmf.2005.8.377
46. Wang, D., Zhao, S., & Liu, Y. (2017). Hipoglycemic and hypolipidemic effects of polysaccharide from flower buds of Lonicera japonica in streptozotocin-induced diabetic rats. *International Journal Of Biological Macromolecules*, *102*(1), 396–404.
47. Shrestha, N., Bhatt, N., Neopane, P., Dahal, S., Regmi, P., Khanal, M., & Shrestha, R. (2017). Hepatic Involvement with elevated liver enzymes in Nepalese subjects with type 2 diabetes mellitus.Int. *J Biochem Res Rev*, *16*(1), 8.
48. Ohaeri, O. C. (2001). Effect of garlic oil on the levels of various enzymes in the serum and tissue of streptozotocin diabetic rats. *Bioscience Reports*. https://doi.org/10.1023/a:1010425932561
49. Jiang, Y., Wang, L., Zhang, L., Wang, T., Zhou, Y., Ding, C., Yang, R., Wang, X., & Yu, L. (2015). Extraction and antioxidant activity of polysaccharides from Salvia miltiorrhiza Bunge residue. Int. J. Biol. Macromol. https://doi.org/.
50. 1016/j.ijbiomac.2015.05.024.
51. Rahimi, P., Ghasemi, E., Esmaeili, D., & Hekmati, M. (2025). Synthesis of ficus carica sap-functionalized Nano-chitosan for biomedical applications: apoptosis induction and tumor cell line growth Inhibition. Results Chem. https://doi.org/.
52. 1016/j.rechem.2025.102115.
53. Islam, T., Ganesan, K., & Xu, B. (2019). New Insight into mycochemical profiles and antioxidant potential of edible and medicinal mushrooms: A review. *Int J Med Mushrooms*. https://doi.org/10.1615/intjmedmushrooms.2019030079
54. Zhang, T., Jayachandran, M., Ganesan, K., & Xu, B. (2018). Black true aqueous extract attenuates oxidative stress and inflammation in STZ-induced hyperglycemic rats via Nrf2 and NF-_B pathways. Front. Pharmacol. https://doi.org/.
55. 3389/fphar.2018.01257.

# Figures

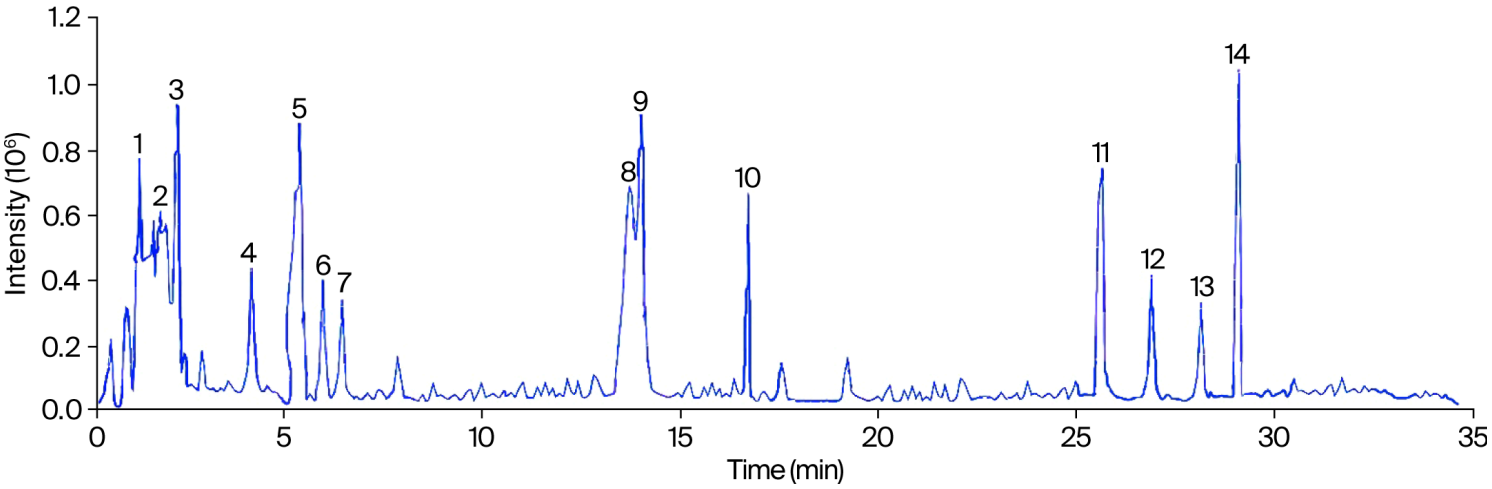



**Figure 1**

Chromatographic profile of phenolic constituents from pink pepper (*Schinus terebinthifolius* Raddi) extract obtained by HPLC coupled with UV and MS detection. The separation highlights distinct peaks corresponding to individual phenolic compounds, whose identities were confirmed through UV absorption spectra and mass fragmentation patterns. This combined approach allows both qualitative characterization and quantitative assessment of the phenolic composition in the extract.

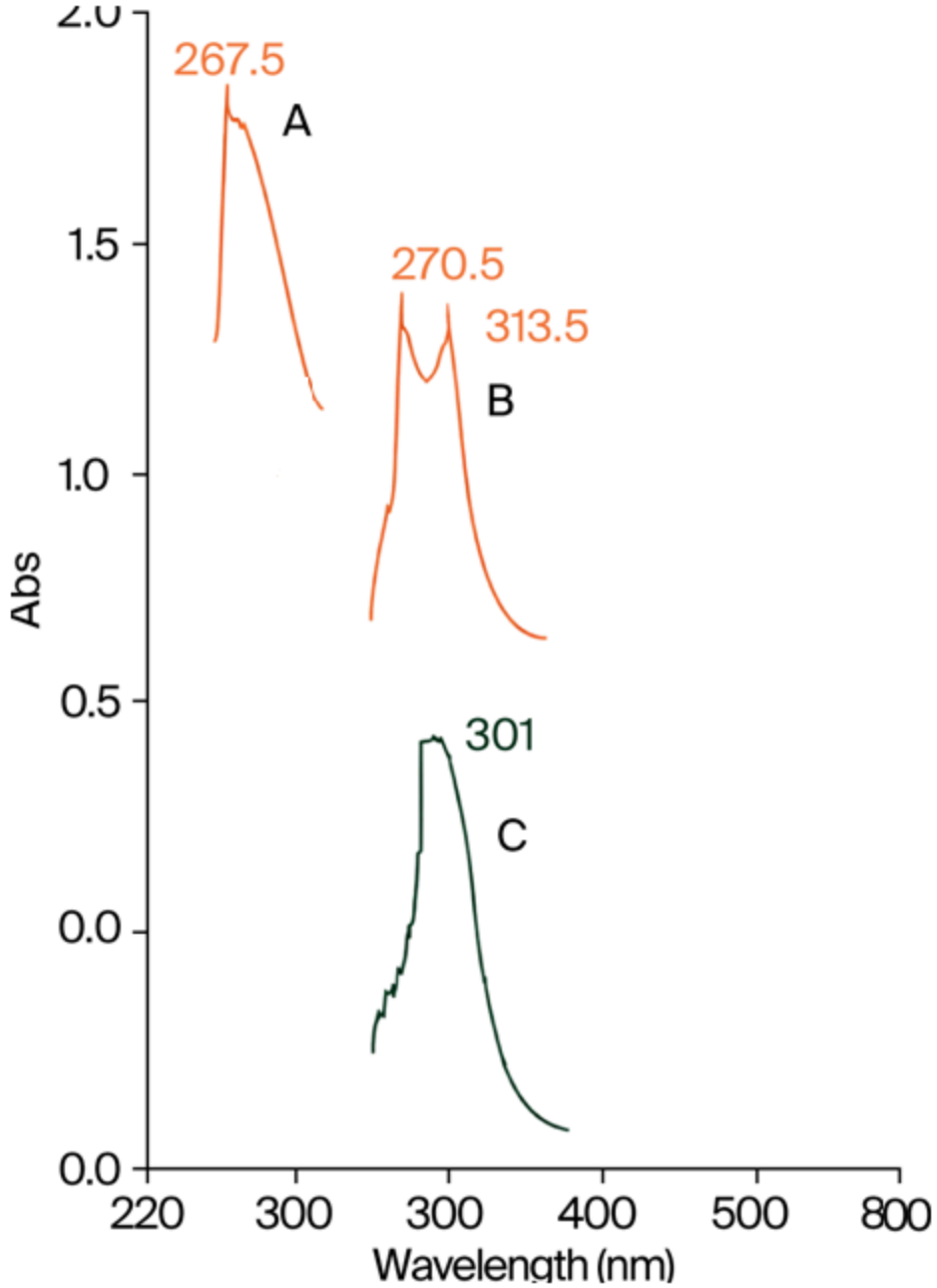



**Figure 2**

“The UV–Vis spectra illustrate distinct profiles for 267.5 nm (A) STCeriaNPs, 270.5 and 313.nm5(B) the ST extract, and 301 nm(C) pure CeriaNPs. Spectrum A exhibits new absorption peaks and noticeable band shifts relative to B and C, reflecting the binding of phytochemicals from the extract to the cerium oxide surface. These spectral changes serve as clear confirmation of the successful synthesis of STCeriaNPs

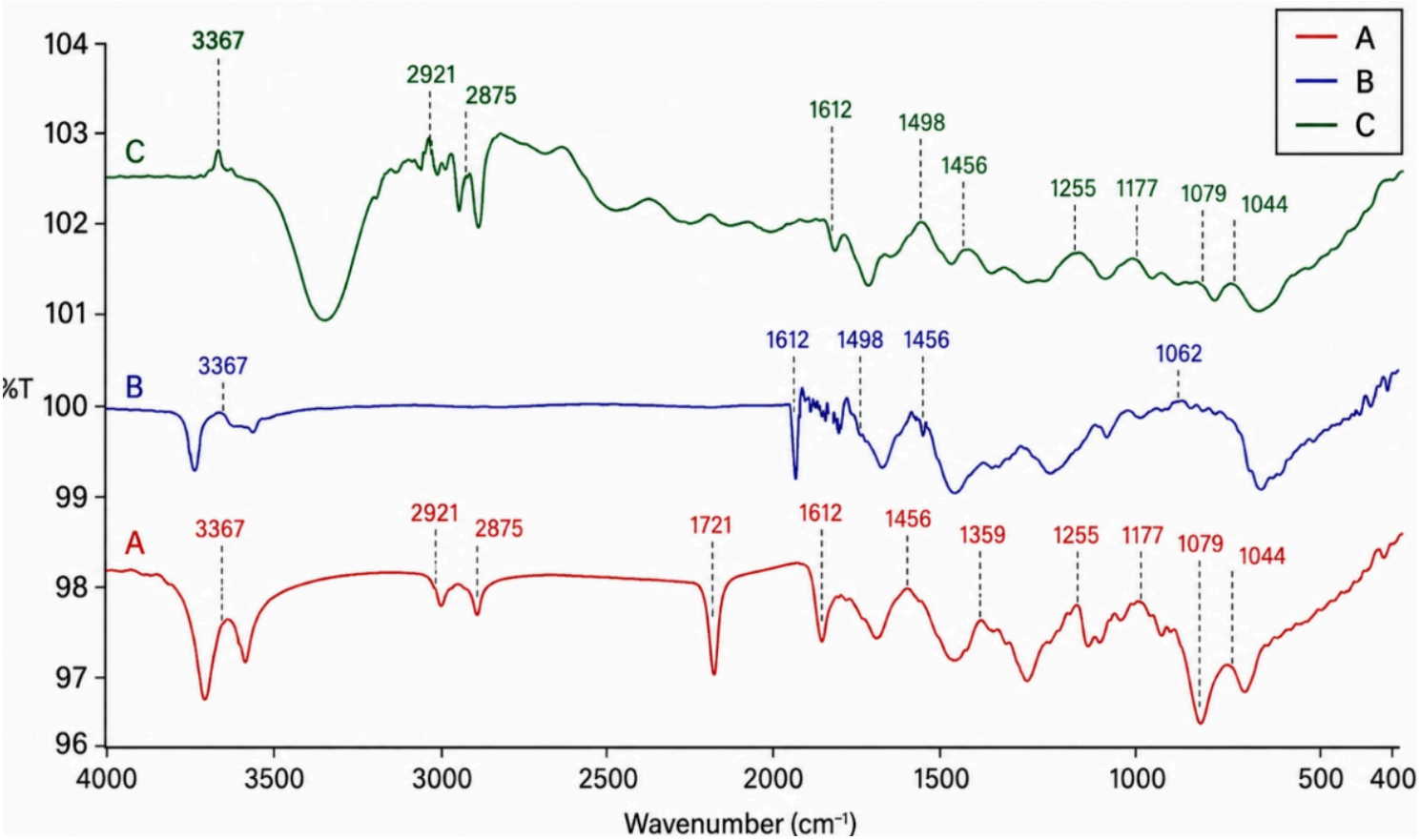



**Figure 3**

FTIR spectra showing the characteristic vibrational bands of (A) Ceria nanoparticles (CeriaNP), (B) the ST plant extract, and (C) the CeriaNPs functionalized with the ST extract (ST–CeriaNP). The comparison highlights the distinct absorption peaks of each component and the shifts or overlaps observed in the composite spectrum, confirming the interaction between the nanoparticles and the extract.

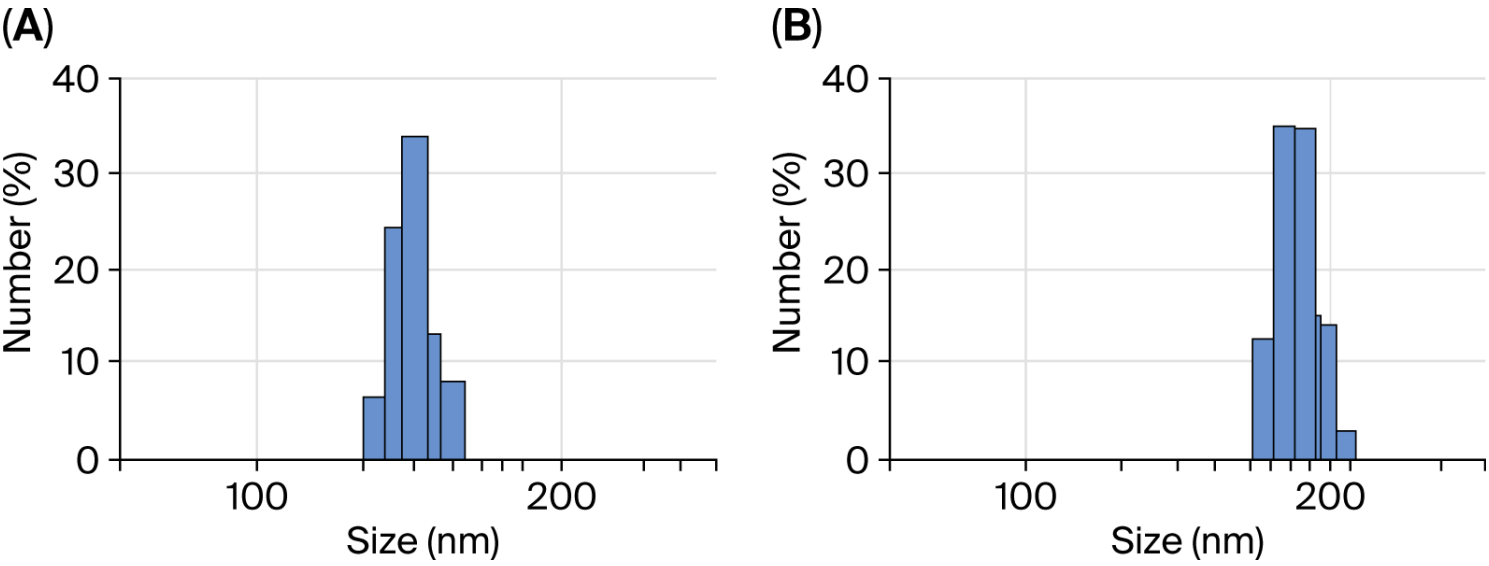
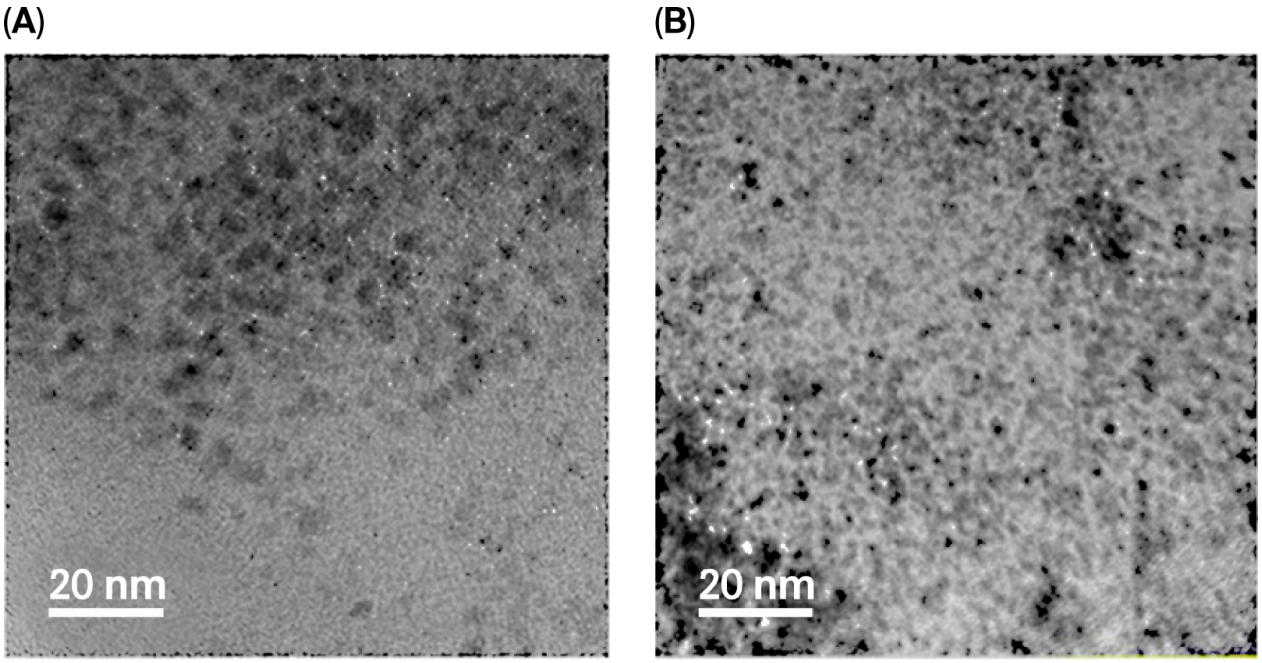
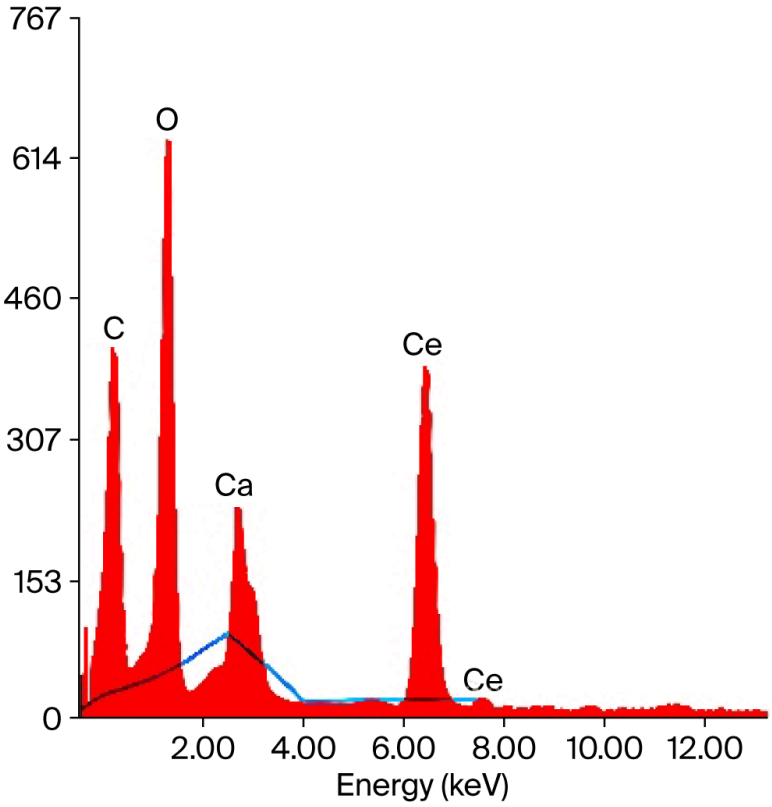



**Figure 4**

Particle Size Distribution (A) Ceria NP display a relatively narrow size distribution, reflecting their native morphology. (B) STCeria NP exhibits a broader and shifted distribution, consistent with surface tailoring effects that alter particle aggregation.




(C)




| Element | % |
|---|---|
| C | 39.99 |
| O | 29.42 |
| Ce | 14.94 |
| Ca | 13.61 |

**Figure 5**

Characterization of synthesized nanoparticles. (A) Transmission electron microscopy (TEM) image of STCeriaNP, showing spherical (B) TEM image of the composite ST/STCeriaNP, where the ceria nanoparticles (20 nm) are embedded within the starch matrix, indicating successful incorporation and stabilization. (C) X-ray diffraction (XRD) pattern of STCeriaNP, confirming the crystalline nature of the cerium oxide nanoparticles and the presence of characteristic diffraction peaks consistent with the fluorite structure of ceria

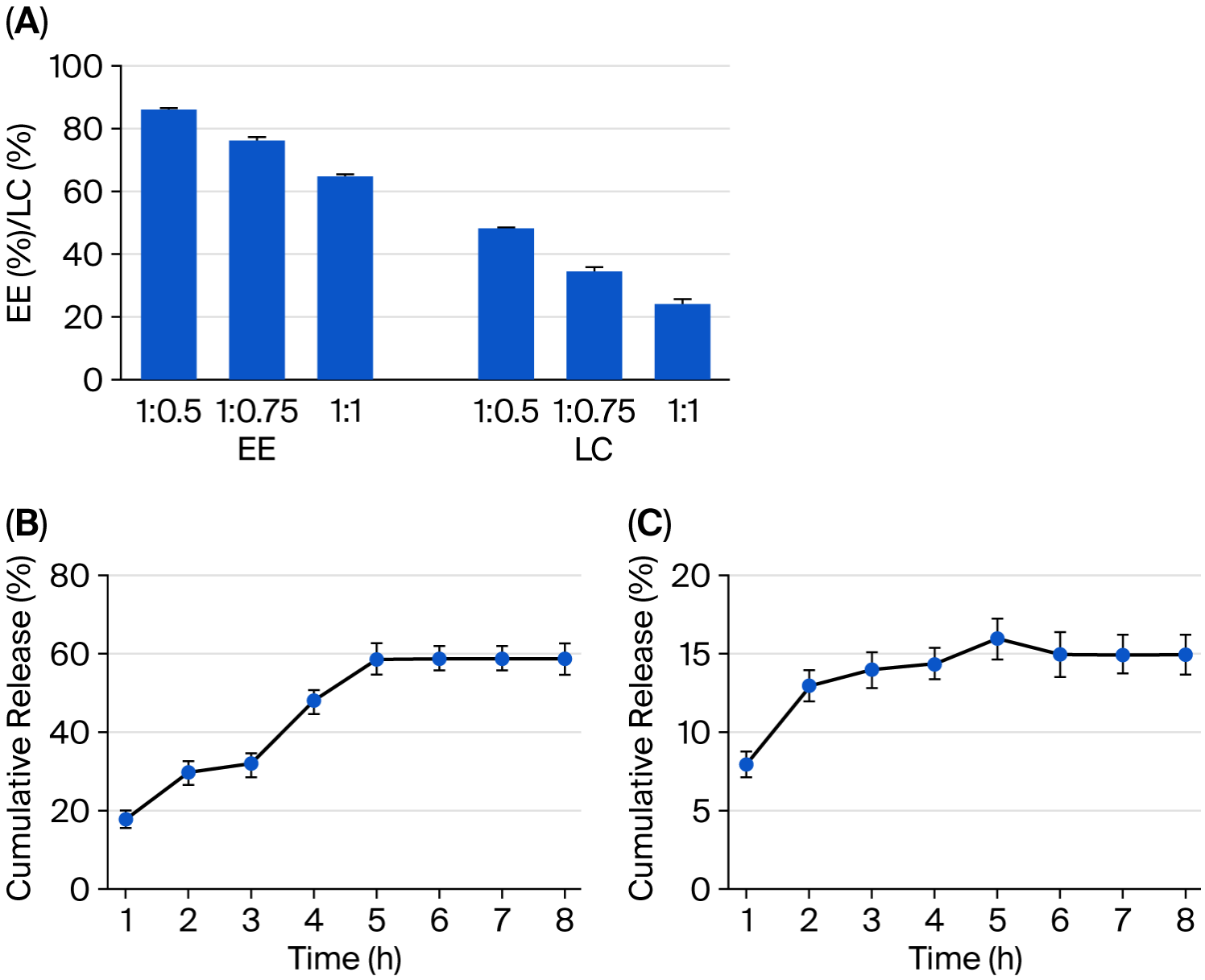



**Figure 6**

(A) Encapsulation efficiency (EE), loading capacity (LC), and ST content of ST-loaded ceria nanoparticles (STCeria NPs) at different Ce/ST weight ratios. (B–C) In vitro release profiles of ST from STCeria NPs under varying pH conditions: pH 5.5 (B), pH 6.5 (B), and pH 7.4 (C).Sustained release (ST) profile at different pH conditions. Panel (A) shows the release behavior at acidic pH 5.5, simulating endosomal or lysosomal environments. Panel (B) illustrates release at mildly acidic pH 6.5, representative of tumor

microenvironments. Panel (C) depicts release at physiological pH 7.4, corresponding to normal extracellular conditions. Together, these profiles highlight the pH-dependent release characteristics of ST, demonstrating how the system responds differently under acidic versus neutral conditions

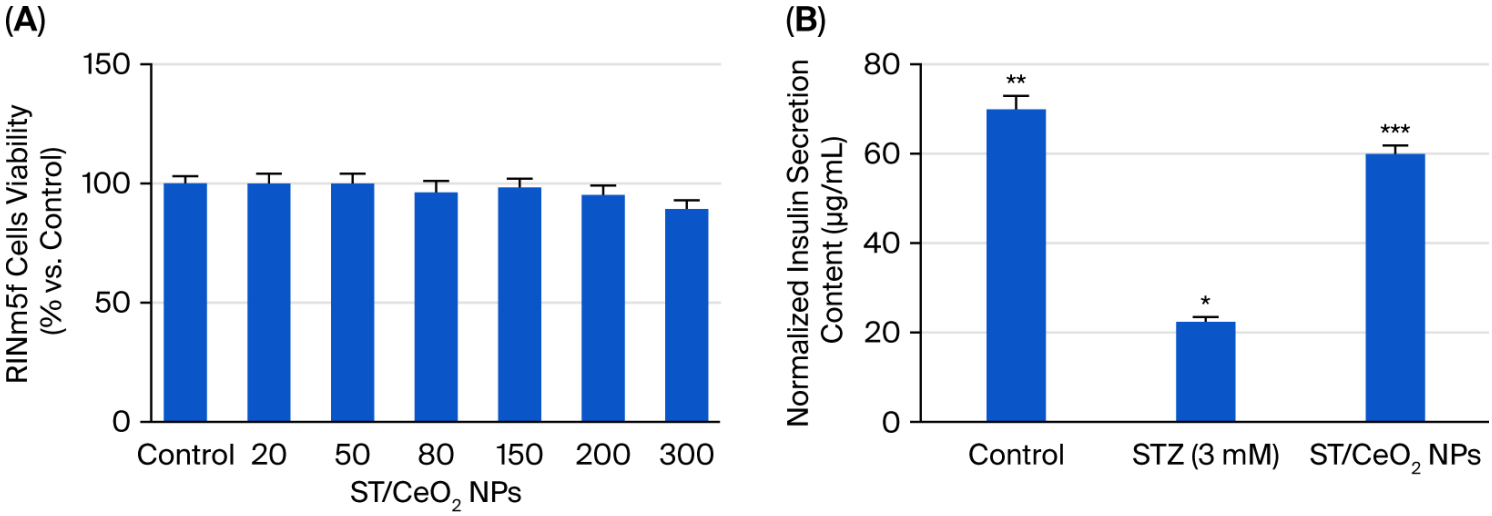



**Figure 7**

Effect of STCeriaNP on RINm5f Beta Cell Viability and Insulin Expression (A) Cell viability of RINm5f beta cells exposed to increasing concentrations of STCeriaNP (0–300 µg/mL). (B) Insulin expression in RINm5f beta cells challenged with 3 mM STZ and subsequently treated with STCeriaNP. Data are presented as mean ± standard deviation (n = 3). Statistical significance was determined relative to untreated controls, with asterisks indicating the level of difference (*p < 0.05; **p < 0.01; ***p < 0.001)

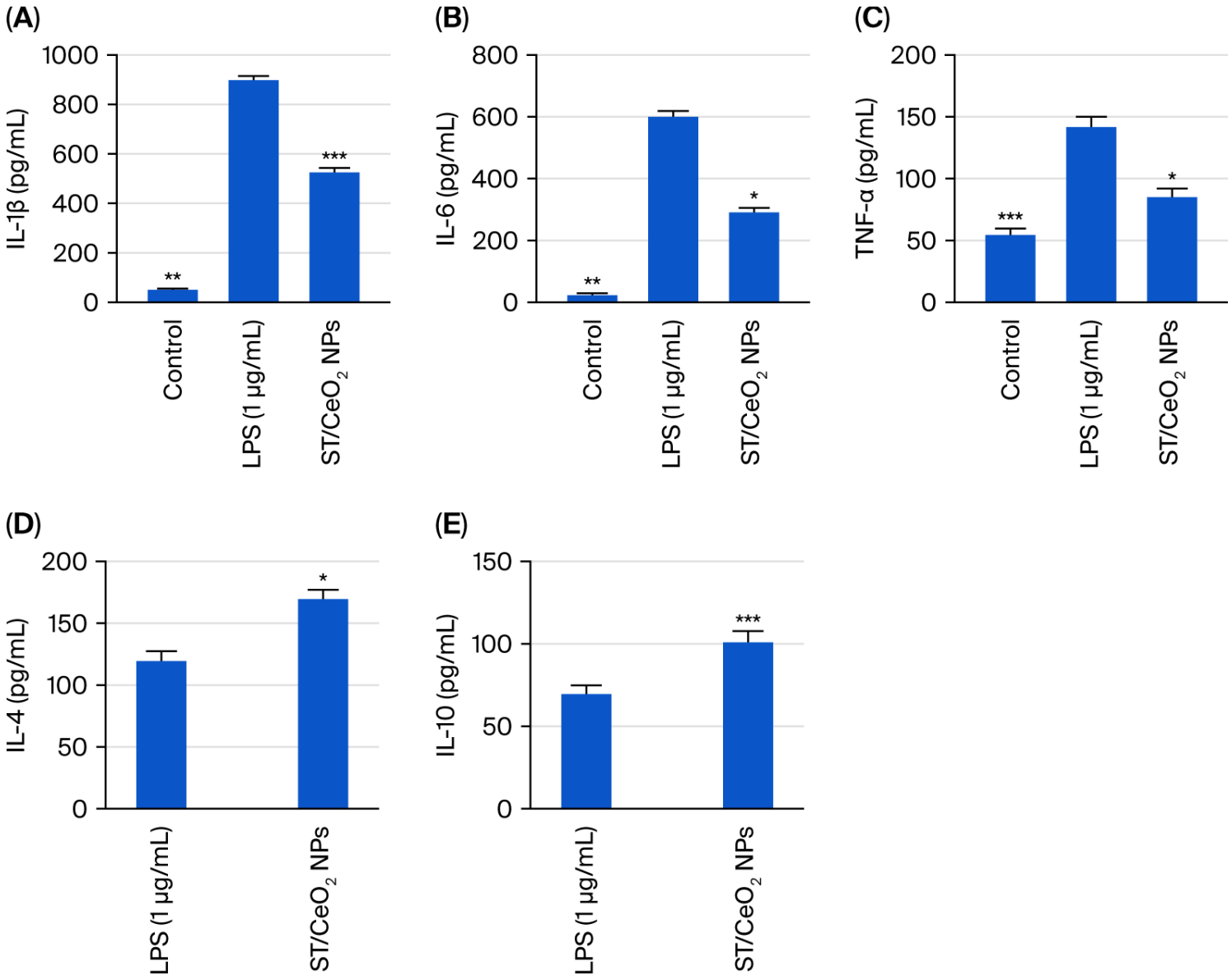



**Figure 8**

Modulation of Cytokine Production by STCeria Nanoparticles in LPS-Stimulated RAW 264.7 Cells. Panels show the effect of STCeria NP treatment on (A) IL-1β, (B) IL-6, (C) TNF-α (proinflammatory cytokines), and (D) IL-4, (E) IL-10 (anti-inflammatory cytokines). Cells were stimulated with LPS to induce an inflammatory response, and cytokine levels were measured after treatment. Data are expressed as mean ± SD (n = 3). Asterisks indicate statistically significant differences compared with untreated controls (*p < 0.001)

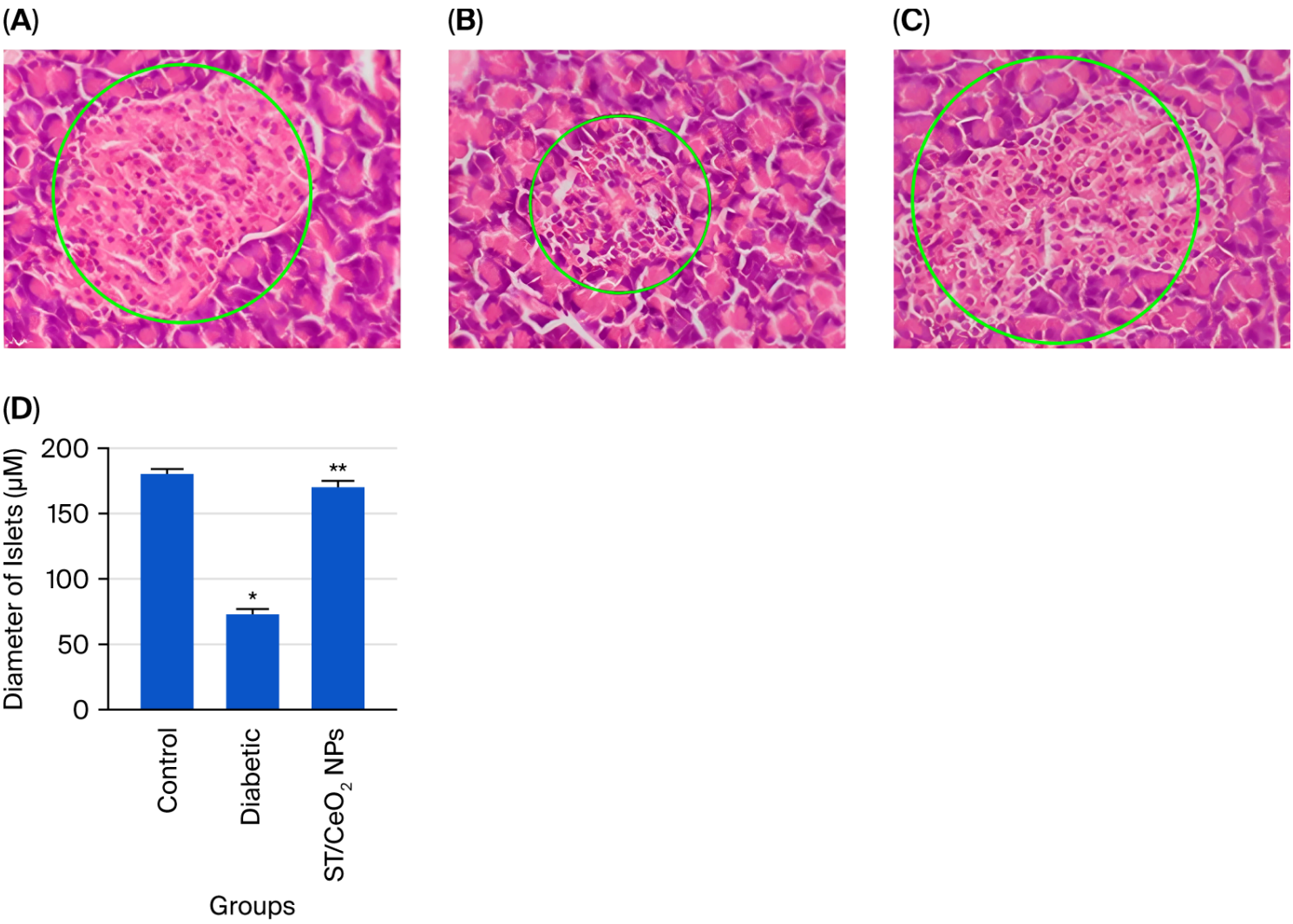



**Figure 9**

Effect of STCeriaNP on pancreatic tissue (H&E staining, X400): (A) Normal pancreas showing intact islet architecture and abundant β-cells (highlighted in green). (B) Diabetic pancreas with marked reduction in islet size and β-cell population (green circle), reflecting impaired insulin-producing capacity. (C) Diabetic mice treated with STCeriaNP exhibit restoration of islet morphology and recovery of functional β-cells (green circle), indicating the therapeutic potential of STCeriaNP in reversing pancreatic damage.

## Supplementary Files

This is a list of supplementary files associated with this preprint. Click to download.

- Tabla5.docx
- Table1.docx
- Table6.docx
- Table4.docx
- Table3.docx

- Table2.docx